Climate Dynamics manuscript No.
(will be inserted by the editor)

Understanding the double peaked El Niño in coupled GCMs

Felicity S. Graham · Andrew T. Wittenberg · Jaclyn N. Brown · Simon J. Marsland · Neil J. Holbrook

Received: date / Accepted: date

Abstract Coupled general circulation models (CGCMs) simulate a diverse range of El Niño-Southern Oscillation (ENSO) behaviors. "Double peaked" El Niño events - where two separate centers of positive sea surface temperature (SST) anomalies evolve concurrently in the eastern and western equatorial Pacific - have been evidenced in Coupled Model Intercomparison Project version 5 (CMIP5) CGCMs and are without precedent in observations. The characteristic CGCM double peaked El Niño may be mistaken for a central Pacific warming event in El Niño composites, shifted westwards due to the cold tongue bias. In results from the Australian Community Climate and Earth System Simulator coupled model, we find that the western Pacific warm peak of the double peaked El Niño event emerges due to an excessive westward extension of the climatological cold tongue, displacing the region of strong zonal SST gradients towards the west Pacific. A coincident westward shift in the zonal current anomalies reinforces the western peak in SST anomalies, leading to a zonal separation between the warming effect of zonal advection (in the west Pacific) and that of vertical advection (in the east Pacific). Meridional advection and net surface heat fluxes further drive growth of the western Pacific warm peak. Our results demonstrate that understanding historical CGCM El Niño behaviors is a necessary precursor to interpreting projections of future CGCM El Niño behaviors, such as changes in the frequency of eastern Pacific El Niño events, under global warming scenarios.

F. S. Graham
Institute for Marine and Antarctic Studies, University of Tasmania, Private Bag 129, Hobart, Tasmania 7001, Australia.
Tel.: +61 3 6226 6379
E-mail: fsm@utas.edu.au

A. T. Wittenberg
National Oceanic and Atmospheric Administration, Geophysical Fluid Dynamics Laboratory, Princeton, USA

J. N. Brown
CSIRO, Oceans and Atmosphere, Hobart, Tasmania, Australia

S. J. Marsland
CSIRO, Oceans and Atmosphere, Aspendale, Victoria, Australia

N. J. Holbrook
Institute for Marine and Antarctic Studies, University of Tasmania, Hobart, Tasmania, Australia; ARC Centre of Excellence for Climate System Science, Hobart, Tasmania, Australia

Keywords El Niño evolution · coupled general circulation model · CMIP5 · cold tongue bias · climate change

1 Introduction

Coupled General Circulation Models (CGCMs) are among our most effective tools for investigating the dynamics of El Niño-Southern Oscillation (ENSO) and the response of ENSO to global warming (Meehl et al, 2006; Yeh et al, 2006, 2009; Collins et al, 2010; Vecchi and Wittenberg, 2010). Improvements are continually being made to these models to better represent the salient features of ENSO, such as its amplitude, frequency, seasonality, and stability (AchutaRao and Sperber, 2006; Guilyardi et al, 2009; Deser et al, 2012; Guilyardi et al, 2012, 2013; Bellenger et al, 2014; Kim et al, 2014; Guilyardi et al, 2015). Nevertheless, there is considerable diversity in the simulation of ENSO dynamics, both within and across CGCMs (Capotondi et al, 2006; Lloyd et al, 2009; Belmadani et al, 2010; Ham and Kug, 2012; Lloyd et al, 2012; Brown et al, 2013; Capotondi, 2013; Capotondi et al, 2015a,b; Choi et al, 2015) and even more diversity in how ENSO will change under global warming (Leloup et al, 2008; Guilyardi et al, 2009; Collins et al, 2010; Boucharel et al, 2011; Kim and Jin, 2011; DiNezio et al, 2012; Watanabe et al, 2012; Taschetto et al, 2014; Latif et al, 2015).

It follows that a current focus of ENSO research is in quantifying the realism of behaviors simulated by CGCMs, which requires comparison of model output with observed features such as sea surface temperature (SST), winds, rainfall, clouds, mixed layer depth, thermocline depth, and ocean currents. However, we have glimpsed only a sample of the possible ENSO behaviors and spatial diversity that could occur (figure 1). This is at least partly due to the fact that ENSO modulates climate on multiple timescales, demonstrating strong interannual variability as well as decadal to multidecadal variability (Allan, 2000; Allan et al, 2003; Wittenberg, 2009; Kug et al, 2010; Choi et al, 2012; Ogata et al, 2013; Meehl et al, 2013; Holbrook et al, 2014; Lee et al, 2014; Wittenberg et al, 2014; Wittenberg, 2015), and such long-term variability may not yet be clearly distinguishable from our relatively short observational record. The framework schematized in figure 1 presents three of the possible scenarios for the range of ENSO behaviors evidenced in CGCMs: i) CGCMs simulate realistic behaviors, of which some may mirror the observations; ii) CGCMs are unable to simulate present-day ENSO behaviors; or iii) CGCMs capture behaviors that are qualitatively similar to those of the real world as well as some unrealistic ones. [Additional scenarios to these three discussed here are possible, such as the observational or reanalysis data exhibiting biases in their representation of reality, as well as the real-world variability changing due to external radiative forcings.] Scenario i) is desirable if we are to use CGCMs to understand future externally forced ENSO events, while scenario ii) implies little faith in the ability of coupled models to perform this task. Based on results from recent studies (e.g. Wittenberg et al, 2006; Guilyardi et al, 2009; Brown et al, 2013) scenario iii) is perhaps the most likely, indicating that while CGCMs are useful, their underlying biases should be taken into consideration when interpreting simulated ENSO behaviors.

Observations suggest that there is a continuum of El Niño spatial diversity in warming, with centers of action located from the eastern equatorial Pacific to the central equatorial Pacific (Giese and Ray, 2011; Johnson, 2013; Capotondi et al, 2015b). A recent trend classifies El Niño events as "eastern Pacific" events or "central Pacific" events depending on the location of maximum sea surface temperature warming at the height of the El Niño event (Ashok et al, 2007; Kao and Yu, 2009; Yeh et al, 2009; Lee and McPhaden, 2010; Yu and Kim, 2013; Yeh et al, 2014). [Although, these classifications are qualitative descriptors of diversity, rather than being indicative of different modes of spatial variability; Capotondi et al, 2015b.] Nevertheless, the patterns of warming simulated by CGCMs do not necessarily closely align with those of observations or flux-forced ocean general circulation models (OGCMs). For instance, while observations and OGCMs show strong, and relatively continuous, variability in SST anomalies (SST') along the equator from the central to the eastern Pacific, the pattern of SST' in CGCMs is split into two separate centers of action, in the western-central and eastern Pacific (figure 2). The western-central Pacific peak of warm SST' in figure 2, or indeed in composites of El Niño SST', might be interpreted as the CGCM analog of the central Pacific El Niño event, whose center of action is shifted westwards due to the cold tongue bias (Wittenberg et al, 2006; Kao and Yu, 2009; Yeh et al, 2009; Ham and Kug, 2012; Taschetto et al, 2014). However, systematic inspection of the evolution of CGCM El Niño events reveals a "double peaked" pattern of warming in CGCMs - with two warm peaks developing concurrently in the eastern and central Pacific (e.g., figure 3). This double peaked El Niño event is common in Coupled Model Intercomparison Project version 5 (CMIP5) CGCMs (figure 4). A double peaked structure was also evident in the SST' variance of CMIP3 models, e.g., the CSIRO-Mk3.0 model (figure 1 of Capotondi et al, 2006).

The spatial structure of SST' is essential for determining the atmospheric response to ENSO. This is especially the case near the convectively-active region of the western Pacific warm pool, where subtle variations in SST can have large impacts on the location and intensity of atmospheric latent heating, and thereby the global atmospheric circulation. This in turn affects not only the feedbacks critical to ENSO (Choi et al, 2013, 2015), but also the structure of the atmospheric stochastic forcing (Vecchi et al, 2006b; Gebbie et al, 2007), and ENSO's remote teleconnections (Capotondi et al, 2015b; Jia et al, 2015; Yang et al, 2015; Krishnamurthy et al, 2015, 2016; Zhang et al, 2016). Thus it is important to assess and understand the biases that CGCMs have in their spatial pattern of SST' during ENSO, as well as how those biases affect ENSO behavior, remote impacts, and ENSO sensitivities to climate change.

The goal of this paper is to investigate the behavior of the CGCM double peaked El Niño event, including the mechanisms that underlie its development. We further seek to address whether the CGCM double peaked El Niño event is a realistic and likely representation of El Niño spatial diversity, or an artifact of coupled model biases. In section 2 we introduce the data and techniques used to identify and analyze the double peaked El Niño event. Section 3 presents analysis of the double peaked El Niño event in the CMIP5 suite of CGCMs. The dynamics giving rise to the double peaked event dynamics are examined in the context of the Australian Community Climate and Earth System Simulator Coupled Model version 1.3 (Bi et al, 2013a). The results are discussed and summarized in section 4.

2 Data and methods

2.1 CMIP5 CGCMs

We analyze the evolution of SST' during double peaked El Niño events in *pre-industrial control* (*PiControl*) and *historical* simulations of 36 climate models submitted to the Coupled Model Intercomparison Project Phase 5 (CMIP5) database (table 1). The nomenclature of the terms "*PiControl*" and "*historical*" follow Taylor et al (2012). *PiControl* simulations attempt to capture the preindustrial climate equilibrium state and are simulated over several hundreds of years; *historical* simulations represent forced runs using observed atmospheric composition changes (atmospheric forcing from both natural and anthropogenic sources) from the mid-19th Century to near present day.

To diagnose the likely mechanisms underpinning the double peaked El Niño event, monthly anomalies of SST, and all variables analyzed from the Australian Community Climate and Earth

System Simulator (ACCESS) simulation, are computed by subtracting the annual cycle from the monthly mean outputs. The data are smoothed using a 13-point Parzen filter to remove frequencies of sub-annual variability.

2.2 The ACCESS model

To investigate the mechanisms underpinning the CGCM double peaked El Niño events, we analyze a *PiControl* 505-year simulation of ACCESS version 1.3 (ACCESS-CM1.3). The ocean component of the ACCESS-CM1.3 simulation is an OGCM that draws its codebase and most of its configuration from the NOAA Geophysical Fluid Dynamics Laboratory (GFDL) Modular Ocean Model version 4 (MOM4p1) (Griffies, 2009). A full description of the ACCESS component models can be found in Bi et al (2013a) and Bi et al (2013b), and their implementation is described by Dix et al (2014).

ACCESS-CM1.3 has been tested against various benchmarks important for the simulation of ENSO, finding that its performance and the magnitude of its model biases are comparable to other CMIP5 models (Brown et al, 2013; Rashid et al, 2013a,b; Kim et al, 2014; Taschetto et al, 2014; Rashid and Hirst, 2015). The mean state and biases of the simulated tropical Pacific in ACCESS-CM1.3 are further discussed in appendix A. The ocean component of ACCESS-CM1.3 was previously analyzed in Graham et al (2015).

2.3 Defining El Niño events

El Niño events are defined when a 5-month running mean of the unfiltered SST' in the Niño-3.4 region (5°S-5°N, 170-120°W) exceeds 0.4°C for a period of at least 6 months (Trenberth, 1997). If a single center of SST' warming is isolated to the eastern equatorial Pacific (east of approximately 160°W), the event is classified as an eastern Pacific El Niño. The following method is used to distinguish double peaked El Niño events. Locations of maximum warming along the equator (2°S-2°N) are determined from the centers of warming that enclose SST' of a critical threshold - here, at least 75% of the maximum SST' - for the 2 years surrounding the peak of each El Niño event. El Niño events may be “double peaked” when two separate, concurrently growing, centers of warming are identified in the evolution of the equatorial SST' that each exceed the critical threshold. The two peaks must be separated by cooler SST'. This definition allows us to distinguish between an El Niño event that evolves by propagation from east to west versus one in which the two peaks develop concurrently.

2.4 The mixed layer heat budget

The mixed layer heat budget equation used in this study is adapted from Vialard et al (2001) and is given by

$$\partial_t T' = A'_x + A'_y + A'_z + Q' + DER', \tag{1}$$

where the symbol ∂_t represents a partial derivative with respect to time, the apostrophe $'$ denotes an anomalous quantity, and T' is the anomalous potential temperature integrated over the mixed layer. The term A'_x on the right-hand side represents the mixed layer averaged anomalous zonal advection defined as

$$A'_x = -\frac{1}{h}\int_{-h}^{0} \left[\overline{u^*}\partial_x T^{*\prime} + u^{*\prime}\partial_x \overline{T^*} + u^{*\prime}\partial_x T^{*\prime}\right] dz, \tag{2}$$

where u^* is the 4-dimensional zonal current, T^* is the 4-dimensional potential temperature, and the overline notation denotes a climatological quantity. The terms A'_y and A'_z in Eq. (1) represent anomalous meridional and vertical advection, respectively, and are constructed similarly to Eq. (2). The vertical velocity used to calculate A'_z is taken directly from the model output. Q' in Eq. (1) is the anomalous net surface heat flux, which can be calculated by summing the surface shortwave and longwave radiation, and latent and sensible heat fluxes, and subtracting the net shortwave radiation contribution that penetrates through the mixed layer (Q_{swout}). Q' is scaled by the mixed layer depth (MLD, h), the constant specific heat capacity of seawater ($c_p = 3989.24$ J kg^{-1} K^{-1}), and a constant density of seawater ($\rho_0 = 1035$ kg m^{-3}). The term DER' in Eq. (1) represents anomalous residual processes, such as diffusion, turbulent heat fluxes, and entrainment into the mixed layer, that are not well resolved when the heat budget is calculated offline. The time-varying MLD over which the terms are averaged is denoted h, and is defined as the depth at which the density layer σ_t deviates from surface values by 0.125 kg m^{-3} (calculated offline). Derivatives are computed using centered differences. All heat budget calculations are performed on monthly mean output of u, v, w, T, and h.

An offline calculation of the heat budget equation may lead to some terms being over- or underestimated, particularly nonlinear or eddy-related terms. For example, tropical instability waves (TIWs) that are important for the damping of SST' in the eastern equatorial Pacific on seasonal to interannual timescales require sub-monthly resolution to be adequately quantified (Vialard et al, 2001). The closure between $\partial_t T'$ calculated directly from the ACCESS models and the right-hand side of Eq. (1) will be further affected by uncertainties introduced through offline calculations. Finally, the residual term includes heat produced through mixing - a process that is not well-resolved in an offline parameterization. Nevertheless, offline calculation of heat budget terms has been used widely (Zhang et al, 2007; Huang et al, 2010, 2011; Choi et al, 2012; Graham et al, 2014) and is sufficient for our purposes of determining the dominant balance of terms giving rise to the CGCM double peaked El Niño. Eq. (1) and its derivation are described in more detail in Vialard and Delecluse (1998).

In what follows, we refer to the depth-averaged (i.e., 3-dimensional, in time, latitude, and longitude, rather than the asterisked 4-dimensional) forms of the terms on the right-hand side of Eq. (2), and the corresponding terms for A'_y and A'_z. For example, in the case of A'_x, the three terms on the right-hand side of Eq. (2) simplify to $-\overline{u}\partial_x T'$, $-u'\partial_x \overline{T}$, and $-u'\partial_x T'$.

3 Results

3.1 The double peaked El Niño event in CMIP5 CGCMs

The metric described in section 2.3 is applied to *PiControl* and *historical* simulations of 36 CMIP5 models (table 1). Double peaked El Niño events are common in all of the CGCMs during the period over which they are simulated (figure 4). Note that our selection of these 36 CMIP5 CGCMs is not dependent on them simulating a double peaked El Niño event. Several models (e.g., GFDL-ESM2G, ACCESS1-3, IPSL-CM5A-MR, and MPI-ESM-P) have a large number of double peaked El Niño events for both *PiControl* and *historical* conditions, while several others (e.g., FIO-ESM, GISS-E2-R-CC, GISS-E2-R, HadGEM2-CC) have relatively few double peaked El Niño events for both *PiControl* and *historical* conditions.

The evolution of SST' composites during double peaked El Niño events from *historical* simulations of selected CGCMs are compared in figure 3. Despite variations in magnitude and timing of El Niño onset between the CMIP5 CGCMs, in each model two warm peaks in SST' emerge during the first 6 months of the El Niño event. The warm peaks grow simultaneously, and separately, during the onset and development of El Niño.

Compared with *historical* simulations, *PiControl* simulations are systematically biased towards simulating more double peaked El Niño events (figure 4). 86% of the 36 CGCMs simulate a greater proportion of double peaked El Niño events in pre-industrial conditions than in *historical* conditions. The mean fraction of double peaked El Niño events to all El Niño events in *PiControl* simulations is approximately 40.3% compared with 26.2% in *historical* simulations.

The location of the western Pacific warm peak during double peaked El Niño events varies from approximately 140°E to 140°W in the CMIP5 CGCMs. We investigate whether this is related to the magnitude of the cold tongue bias, which has been found to extend El Niño-related warming in CGCMs further westwards than observed (Taschetto et al, 2014). We use the mean location of the dynamic warm pool edge (DWPE) - the isotherm that best captures the maximum in the zonal salinity gradient - as a proxy for the magnitude of the cold tongue bias. This is because CGCMs with stronger cold tongue biases tend to simulate DWPEs further towards the western Pacific warm pool (Brown et al, 2013). The relationship between the cold tongue bias and the location of the western Pacific warm peak during double peaked El Niño events in the CMIP5 CGCMs is illustrated in figure 5. A clear pattern emerges: during double peaked El Niño events, models with stronger cold tongue biases also simulate western Pacific warm peaks located further towards the western Pacific warm pool. Furthermore, models that simulate more double peaked El Niño events tend to have DWPEs shifted further west than models with fewer double peaked El Niño events: 14 of the 20 models with the highest fraction of double peaked events simulate a DWPE west of the median (≈170°E). This relationship corroborates our earlier result that the fraction of double peaked El Niño events is greater in *PiControl* simulations, where the cold tongue is strengthened relative to *historical* conditions due to a relative decrease in atmospheric CO_2 concentrations (Vecchi et al, 2006a; Collins et al, 2010; Vecchi and Wittenberg, 2010; Watanabe et al, 2012). However, this relationship is not necessarily indicative of the full extent of the cold tongue bias in the model. That is, figure 5 only incorporates the double peaked events that meet the criterion outlined in section 2.3; it does not take into account models that simulate other spatial patterns of El Niño that have not been evidenced in the observational record (e.g., both CSIRO-Mk3-6-0 and CNRM-CM5 simulate El Niño events evolving exclusively in the western Pacific warm pool) and might be a result of the cold tongue bias, or indeed other biases, in coupled models.

We found earlier that double peaked El Niño events are more prevalent in *PiControl* simulations than in *historical* simulations. Given the importance of the DWPE in generating double peaked El Niño events, we test whether the change in fraction of double peaked El Niño events from *PiControl* to *historical* simulations is related to mean state changes. Both the change in the mean longitude of the DWPE (dDWPE), and the fraction of double peaked El Niño events in *PiControl* simulations (F(piC); i.e., the *PiControl* mean state), are predictors for the change in the fraction of double peaked El Niño events from *PiControl* to *historical* (dF). We test the dependence of dF on each of these predictors using multiple linear regression. Considering all subsets of the two predictors, the model that yields the best fit ($R^2 = 0.40$) has the form

$$\mathrm{dF} = a * \mathrm{dDWPE} + b * \mathrm{F(piC)} + c, \tag{3}$$

where a, b, and c are constant coefficients. The parameters from the regression analysis are highlighted in table 2 and the resulting fitted data in figure 6. The *PiControl* mean state, F(piC), is found to have the greatest effect on the change in fraction of double peaked El Niño events simulated.

In what follows, we examine the evolution of heat budget dynamics during double peaked El Niño events in ACCESS-CM1.3. We note that it is possible that the CGCM double peaked El

Niño event arises due to different mechanisms in different CMIP5 models; however, analysis of all CMIP5 models is beyond the scope of the current study.

3.2 The double peaked El Niño event in ACCESS-CM1.3

A total of 89 El Niño events are identified in the 505-year *PiControl* simulation of ACCESS-CM1.3. Of the CGCM El Niño events, 65 are classified as double peaked events and 10 as eastern Pacific events. In a further 12 of the remaining events two distinct peaks of warming are present, as in the double peaked El Niño event, but the SST' in either the eastern or western peak does not meet the threshold to allow classification as a double peaked event. SST' for the ACCESS-CM1.3 double peaked and eastern Pacific El Niño events are composited. The significance of the heat budget trends from these composite events is investigated and discussed in appendix B (figure A4).

3.2.1 Heat budget analysis

The heat budget terms from Eq. (1) are analyzed in the ACCESS-CM1.3 *PiControl* simulation to determine the mechanisms giving rise to the western Pacific warm peak of the double peaked El Niño event (figure 7). During the double peaked event, westerly wind anomalies generated near the DWPE (163°E) incite the growth of eastwards zonal current anomalies there. The strong zonal current anomalies occur at the maximum in the mean zonal temperature gradient (Picaut et al, 1996, 1997; Clarke et al, 2000), which is displaced further to the west than observed due to the cold tongue bias (Brown et al, 2013). This leads to the zonal advective feedback $-u'\partial_x\overline{T}$ achieving its maximum near the DWPE, and dominating the growth of the mixed layer temperature anomaly, T', there. Warming induced by the zonal advective feedback then increases the positive anomalous mixed layer temperature gradient in the western Pacific, leading to growth of the mean zonal advection term $-\overline{u}\partial_x T'$ in the western Pacific. The climatological westward flow of the South Equatorial Current, which is up to 0.4 m s^{-1} stronger than observed in the western-central Pacific in the CGCM than in observations (figure 8), advects the western warm patch to the west.

We next investigate how the ACCESS-CM1.3 double peaked El Niño event differs from the eastern Pacific event (figure 7). The western extent of warming extends west of 160°E during both CGCM El Niño events; however, a western warm peak does not develop in the ACCESS-CM1.3 eastern Pacific event, partly due to an eastwards shift in the patterns of westerly wind stresses, which is consistent with previous studies (Rasmusson and Carpenter, 1982; Kalnay et al, 1996; Wittenberg, 2004). That is, during the ACCESS-CM1.3 eastern Pacific El Niño event the maximum in the westerly (i.e., anomalous) equatorial zonal wind stresses is shifted further to the east (150-120°W) than in the ACCESS-CM1.3 double peaked El Niño event (150°E-160°W), and the westerly wind stresses in the region of the western Pacific warm peak (150°E-180°) are weaker by approximately 3.4×10^{-3}N m^{-2} on average during the first 24 months of the eastern Pacific event than the double peaked El Niño event. As a consequence, the zonal advective feedback is smaller by approximately 0.10°C month^{-1} in the western Pacific during the eastern Pacific El Niño event than during the double peaked event, preventing the development of significant warming in the western Pacific. This is consistent with observed El Niño events that develop mainly in the eastern Pacific, the growth of which is typically dominated by the thermocline feedback (Jin, 1997a,b; Yeh et al, 2014). The nonlinear meridional advection term $-v'\partial_y T'$ provides consistent warming throughout the central Pacific during eastern Pacific El Niño events. By contrast, during double peaked events this term is almost negligible in the central

Pacific, but larger ($> 0.15°$C month^{-1}) in the western Pacific, where anomalous meridional temperature gradients are amplified.

The relative contributions of the heat budget terms to the central equatorial Pacific $\partial_t T'$ during the double peaked and eastern Pacific El Niño events are shown in figure 9. Here, the difference between each heat budget term during double peaked and eastern Pacific El Niño events (i.e., the bottom panels in figure 7) in the central equatorial Pacific (defined as the local minimum in SST' variance, 154°W) is subtracted from the difference in the western-central equatorial Pacific (the local maximum in SST' variance, 178°E). The key drivers of the western Pacific warm peak are the zonal advection terms $-u'\partial_x \overline{T}$ and $-u'\partial_x T'$, which are the result of relatively stronger anomalous zonal equatorial currents acting on the zonal temperature gradient at the edge of the western Pacific warm pool. The meridional advection terms $-v'\partial_y T'$ and $-\overline{v}\partial_x T'$ contribute to the growth of $\partial_t T'$ by meridional spreading of the equatorial SST'. The net surface anomalous heat flux Q' grows, rather than damps, the western Pacific warm peak, largely due to a positive bias in the shortwave heat flux attributed to unrealistic SST-cloud interactions in ACCESS-CM1.3 (Rashid and Hirst, 2015). These unrealistic SST-cloud interactions are partly due to a climatological bias in the low cloudiness of ACCESS-CM1.3, associated with an overly strong cold tongue compared with observations, and also partly due to overly strong descending atmospheric motion. A similar result has been found in the GFDL-CM2.1 CGCM (Wittenberg et al, 2006). While residual eddy effects do contribute somewhat to generating the western Pacific warm peak, they are relatively weak compared to zonal advection, meridional advection, and thermodynamic damping contributions.

4 Discussion

Spurious double peaked El Niño events - with two warming peaks developing concurrently in the eastern and western Pacific - were found to be widespread in CMIP5 CGCMs. The location of the western Pacific warm peaks during double peaked El Niño events was correlated with the location of the dynamic warm pool edge (DWPE), a proxy for the magnitude of the cold tongue bias (Brown et al, 2013). The DWPE was as far west as 155°E in CMIP5 models. CGCMs with more westwards located DWPEs tended to simulate more double peaked El Niño events. The consistency in the response of the CMIP5 CGCMs in simulating the double peaked events serves to corroborate the cold tongue bias as playing an important role in generating the double peaked El Niño events, rather than this event representing a realistic "new flavor" of El Niño. Consequently, a reasonable supposition is that the ENSO behaviors present in *PiControl* and *historical* simulations of CGCMs fit within circle iii) in figure 1; that is, they display some qualitatively similar features to those observed, but also simulate some unrealistic ones that are an artifact of climatological CGCM biases.

The mechanisms giving rise to the double peaked event were further investigated in ACCESS-CM1.3. During double peaked El Niño events in ACCESS-CM1.3, the westwards extension of the equatorial Pacific cold tongue region (eastern extent of the western Pacific dynamical warm pool edge) modified the location of peak warming and dynamical behavior in the western Pacific. In particular, the overly intense and westward-extended cold tongue in CGCMs led to two biases that altered the El Niño feedbacks compared with eastern Pacific El Niño events: (i) an excessive climatological zonal temperature gradient ($\partial_x \overline{T}$) in the western equatorial Pacific that was displaced too far west of the strong climatological vertical temperature gradient in the eastern equatorial Pacific; and (ii) atmospheric deep-convective cloudiness that was displaced too far west and off-equator. The westward-shifted $\partial_x \overline{T}$ led to a western displacement of the zonal advective feedback ($-u'\partial_x \overline{T}$) relative to vertical advective feedbacks ($-\overline{w}\partial_z T'$ and $-w'\partial_z \overline{T}$), generating a secondary western equatorial warm peak. In addition, the intense cold tongue displaced the atmospheric convective zones westward and poleward, leading to insufficient damping of this secondary western peak in SST' by cloud shading. These results highlight the importance of a CGCM's climatology to the dynamics and spatial structure of ENSO and motivate further attention to understanding and correcting mean state biases in CGCMs.

Here, we have focused on just one manifestation of CGCM El Niño diversity: the double peaked pattern of SST warming. Given the similarity in mechanisms giving rise to the western Pacific warm peak of the double peaked event and the central Pacific El Niño event (Yeh et al, 2014), it is possible that the double peaked El Niño event could be mistaken for a westwards-shifted central Pacific El Niño, particularly in composite El Niño events. Furthermore, differences between CGCMs can lead to behaviors that have not yet been observed (e.g., the El Niño event that evolves entirely in the western Pacific warm pool in CSIRO-Mk3.6.0). It follows that studies of future ENSO events, such as changes in the frequency of El Niño spatial behaviors under global warming scenarios, should be cautiously interpreted in light of historical representations of El Niño diversity.

Acknowledgements The ACCESS model is supported by the Australian Government Department of the Environment, the Bureau of Meteorology and CSIRO through the Australian Climate Change Science Program, and the NCI Facility at the ANU. FSG was supported by an Australian Postgraduate Award and a CSIRO Wealth from Oceans scholarship. This research makes a contribution to the ARC Centre of Excellence for Climate System Science. The authors thank two anonymous reviewers for their constructive comments that greatly improved the manuscript.

[Appendix A]

The mean state and biases in ACCESS-CM1.3

The mean SST from ACCESS-CM1.3 and SST bias, with respect to the Bureau of Meteorology Research Centre (BMRC) SST reanalyses (Smith, 1995) over the period 1980-2004, is illustrated in figure A1. ACCESS-CM1.3 is up to 1°C cooler than the reanalysis data in the equatorial Pacific cold tongue region (180-100°E), and up to 2°C warmer east of 100°W along the coast of South America. ACCESS-CM1.3 displays a warm bias in the South Pacific, in the region of the South Pacific Convergence Zone, and in the tropical North Pacific (5°N, 160-110°W).

The standard deviation of tropical Pacific SST' is indicative of the spatial diversity in ENSO variability (figure 2). Variability in the eastern equatorial Pacific in ACCESS-CM1.3 is weaker than in the reanalysis data (the difference in standard deviation is up to 0.6°C at approximately 100°W), including $<$ 0.3°C from 160-140°W, and slightly stronger ($>$ 0.2°C) west of 180° longitude in a secondary western peak. Note that the standard deviation of SST' illustrated in figure 2 is qualitatively similar to the leading mode of an EOF analysis of ACCESS-CM1.3 SST', which also displays the double peaked pattern of warming and represents 44% of the SST' variability in ACCESS-CM1.3 (figure not shown).

The annual means of the equatorial surface heat fluxes for ACCESS-CM1.3 are compared with those from the Objectively Analyzed air-sea Fluxes (OAFlux; provided by the Woods Hole Oceanographic Institute (WHOI) OAFlux project, available at http://oaflux.whoi.edu), the TropFlux reanalyses (Kumar et al, 2012), and the Coordinated Ocean-ice Reference Experiments version 2 (CORE-II, which are used to force ACCESS-OM; Griffies et al, 2012) in figure A2. The annual mean equatorial longwave radiation and sensible heat flux simulated by ACCESS-CM1.3 are within the range of uncertainty estimated from OAFlux, TropFlux, and CORE-II. Latent heat fluxes in ACCESS-CM1.3 are up to 46 W m^{-2} less than those of the reanalyses, particularly in the eastern equatorial Pacific. Equatorial shortwave radiation values simulated by ACCESS-CM1.3 in boreal winter are up to 38 W m^{-2} different from TropFlux.

The mean state of the tropical Pacific MLD in ACCESS-CM1.3 and bias with respect to the UK Met Office (UKMO) subsurface ocean temperature and salinity data (Ingleby and Huddleston, 2007) over the period 1980-2005 are compared in figure A3. The ACCESS-CM1.3 MLDs are up to 50m deeper than the UKMO MLDs in bands stretching between 170°E and 150°W north and south of the equator.

[Appendix B]

Significance of the double peaked El Niño event in ACCESS-CM1.3

Here, we investigate whether the composited double peaked El Niño events are significantly different from the composited eastern Pacific El Niño events. First, the double peaked and eastern Pacific El Niño events from the *PiControl* simulation of ACCESS-CM1.3 are randomly separated into two groups, groups a and b, and composited. We name these composites μ_x of sample size n_x, where $x \in \{DP1.3a, DP1.3b, EP1.3a, EP1.3b\}$. We also consider the double peaked El Niño events from the *PiControl* simulation of ACCESS-CM1.0 and separate them into two composites - $\mu_{DP1.0a}$ and $\mu_{DP1.0b}$ - with sample sizes $n_{DP1.0a}$ and $n_{DP1.0b}$, respectively.

The variable for testing the significance of the difference between composites is the Student's t-distribution:

$$t = \frac{\widehat{\mu_x} - \widehat{\mu_y}}{S\sqrt{\frac{1}{n_x} + \frac{1}{n_y}}}, \text{and} \tag{4}$$

$$S^2 = \frac{(n_x - 1)\widehat{\sigma_x^2} + (n_y - 1)\widehat{\sigma_y^2}}{n_x + n_y - 2}, \tag{5}$$

where $n_x + n_y - 2$ is the number of independent observations for the parameter t, and x and y represent the composited El Niño events being tested. The significance value (p-value) from each test case is calculated using a two-sided Student's t-test.

We define a simple test to establish the significance of the El Niño composite events: namely, the double peaked and eastern Pacific El Niño events are significantly different if the following conditions are satisfied during the evolution of the El Niño event (i.e., the first 24 months of the composite):

Test 1: the differences between the DP1.3a and EP1.3a composites are greater than the differences between the DP1.3a and DP1.3b composites;

Test 2: the differences between the DP1.3b and EP1.3b composites are greater than the differences between the EP1.3a and EP1.3b composites;

Test 3: the differences between DP1.3a events from ACCESS-CM1.3 and DP1.0a events from ACCESS-CM1.0 are greater than the differences between the DP1.3a and DP1.3b events from ACCESS-CM1.3; and

Test 4: the differences between DP1.3b events from ACCESS-CM1.3 and DP1.0b events from ACCESS-CM1.0 are greater than the differences between DP1.0a and DP1.0b events from ACCESS-CM1.0.

The random sampling is repeated 100 times and median values for the differences between the composites, t, and p across the samples are calculated. The results for tests 1-4 are illustrated in figure A4.

For test 1, the median difference between DP1.3a and EP1.3a is approximately ± 2 times greater than the difference between DP1.3a and DP1.3b, which is in the range $[-0.37, 0.19]^\circ$C for the 100 samples generated. The differences in DP1.3a and EP1.3a are greater than one standard deviation across the western-central equatorial Pacific during the 12 months prior to the peak of the El Niño event. The greatest differences in the eastern equatorial Pacific occur during the two months prior to and eight months following the peak of the El Niño event. Differences between DP1.3a and DP1.3b across the 100 samples are not statistically significant. A similar result is found for test 2. Even in the *PiControl* simulations, the sample size of eastern Pacific events in ACCESS-CM1.3 is relatively small – 10 in total – such that the difference between EP1.3a and EP1.3b is likely to be biased by individual events.

The results of tests 3 and 4 illustrate that double peaked events from the ACCESS-CM1.3 model are more similar to each other than to events from ACCESS-CM1.0. Again, the median difference between double peaked events within each model simulation is small (within the range $[-0.22, 0.40]^\circ$C for the ACCESS-CM1.0 simulation), while the median differences in double peaked events between the two models are close to $\pm 2^\circ$C during the development of the El Niño event throughout the equatorial Pacific and in the western and eastern Pacific during the decay periods of the El Niño event (the differences are greater than one standard deviation from the mean in each case). These results provide evidence that the composite double peaked and eastern Pacific El Niño events from ACCESS-CM1.3 are sufficiently different to ensure significance in the trends analysis.

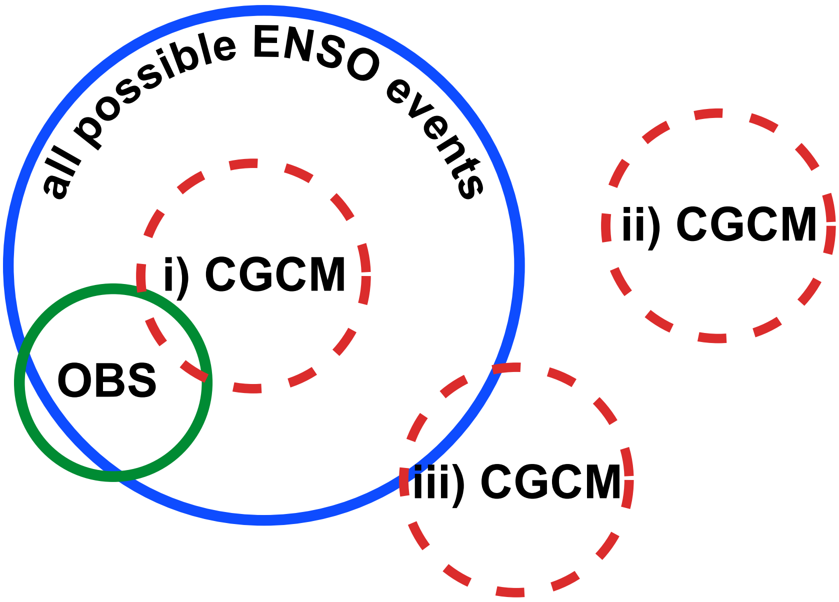

Fig. 1 Venn diagram representing possible relationships between the ENSO behaviors simulated by CGCMs (red dashed circles), the full range of possible ENSO behaviors under present-day conditions (blue circle) and the observed ENSO behaviors (green circle). The green circle extends slightly outside the blue circle to represent observational errors, such as in measurement or reconstruction. We also note that the blue circle is itself evolving on decadal to centennial timescales due to natural internal variability, as well as due to external radiative forcings.

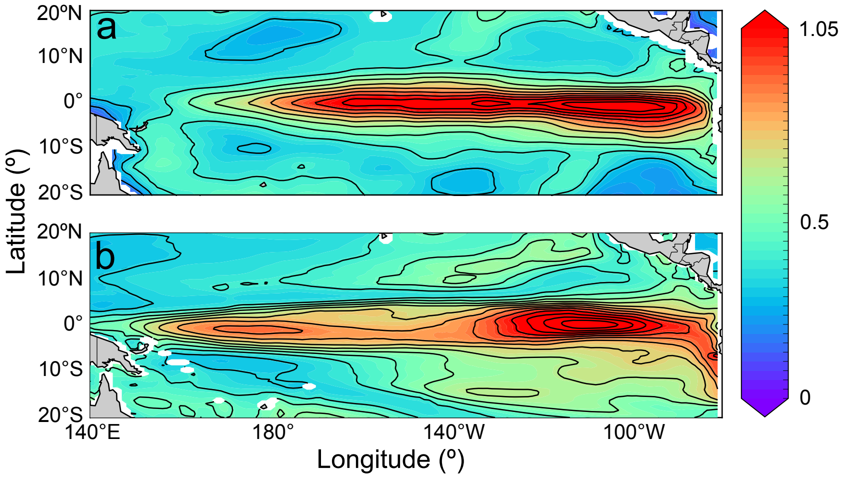

Fig. 2 Standard deviation of sea surface temperature anomalies (shading) in the **a** Bureau of Meteorology Research Centre SST reanalyses (Smith, 1995), and **b** *historical* simulation of ACCESS-CM1.3. Data are in units of °C and the contour interval is 0.025°C. Contours of the standard deviation at the 0.075°C interval are overlaid.

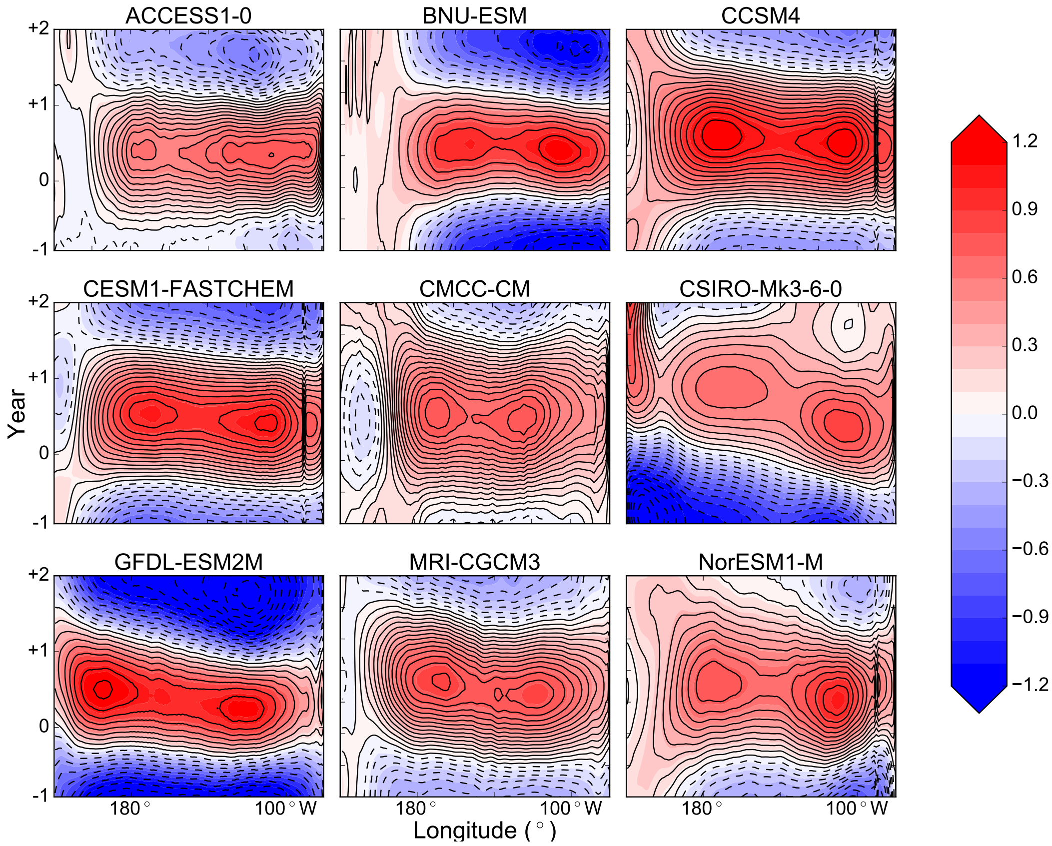

Fig. 3 Examples of the evolution of SST' for the 36 months surrounding composite double peaked El Niño events from *historical* simulations of nine CMIP5 models (as indicated). Data are in units of °C (with contour intervals of 0.1°C) and are averaged over 2°S-2°N.

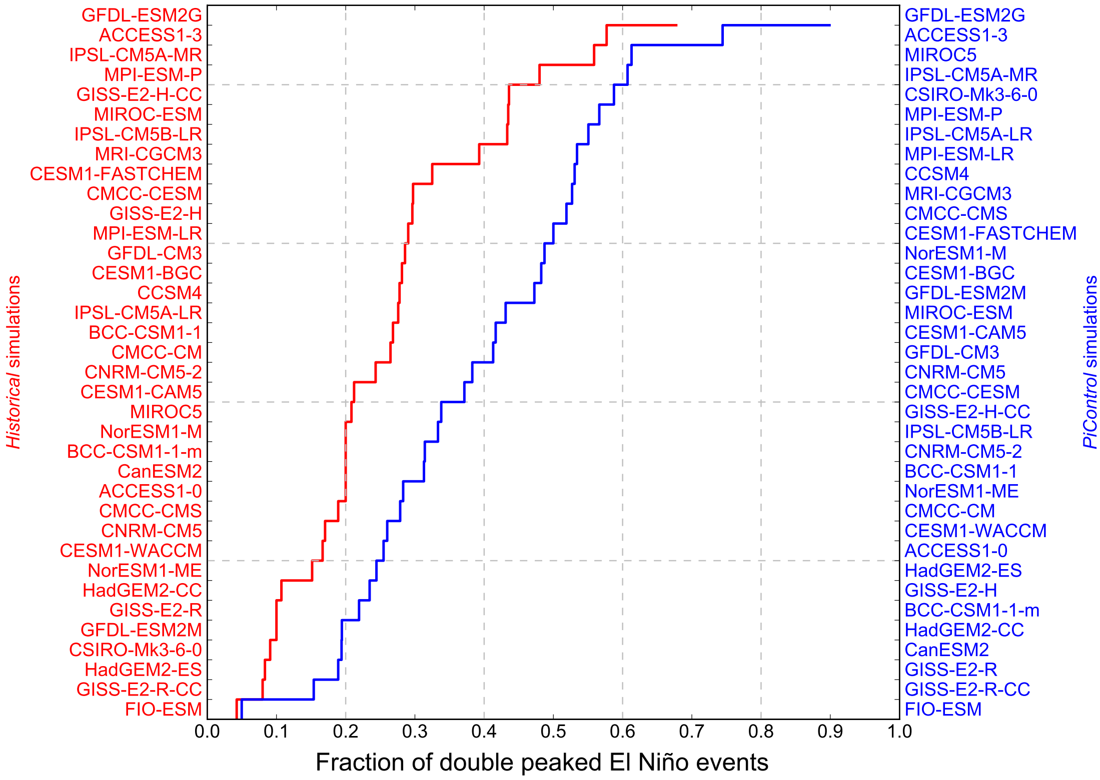

Fig. 4 Fraction of all El Niño events that are classified as double peaked events from *PiControl* and *historical* simulations of 36 CMIP5 CGCMs. Data in blue corresponds to *PiControl* simulations; data in red corresponds to *historical* simulations. The distributions of the *PiControl* and *historical* data are statistically significantly different at the 99% confidence level using a two-side Kolmogorov-Smirnov test (test statistic 0.44, $p = 0.001$).

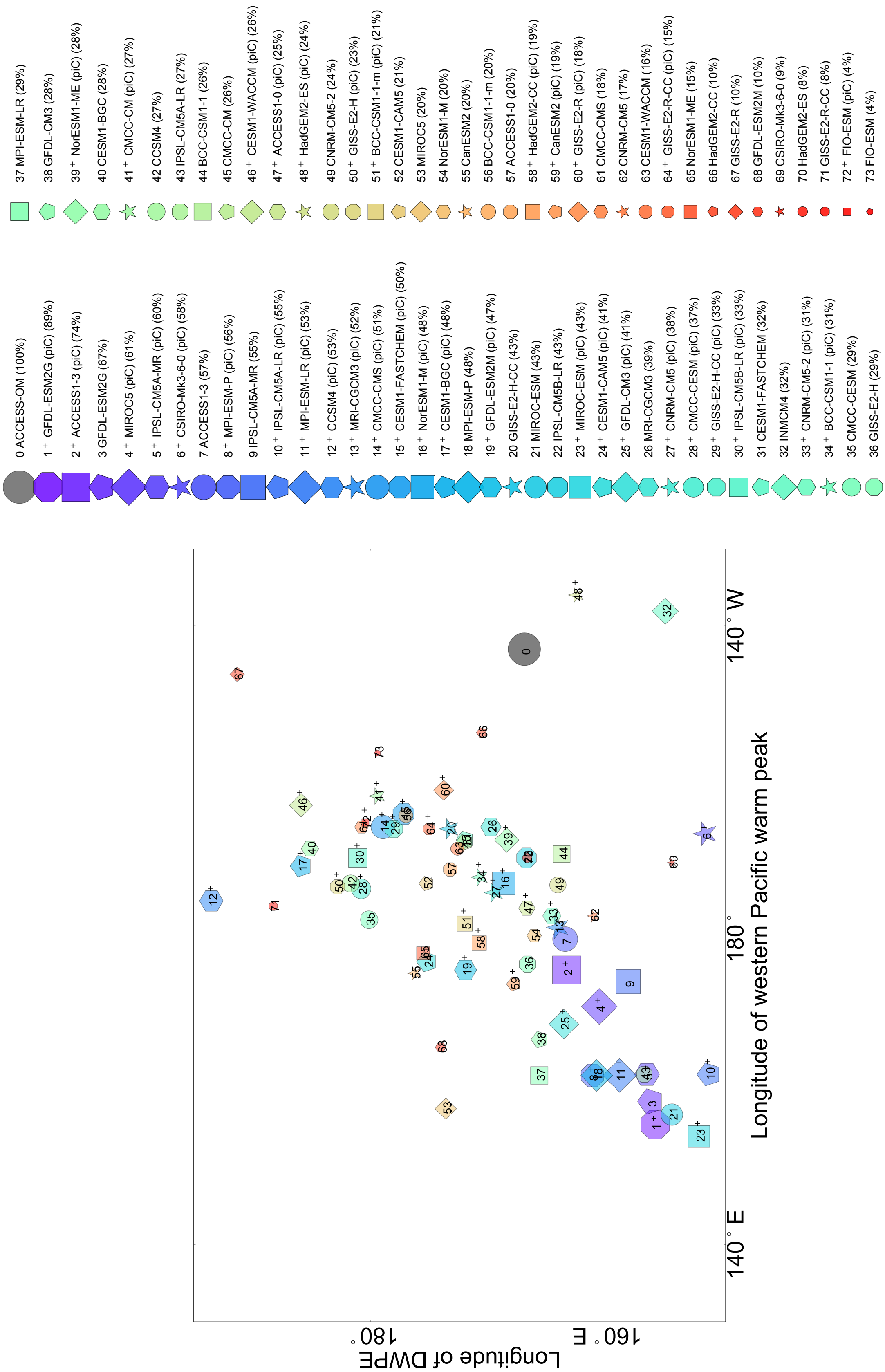

Fig. 5 Mean position of the western Pacific warm peak in a composite double peaked El Niño year versus the mean position of the dynamic warm pool edge in *PiControl* and *historical* simulations of 36 CMIP5 CGCMs. Markers representing each CGCM are sized by the fraction of double peaked events to the total number of El Niño events (see table 1). The large grey circle represents the mean longitude of a composite eastern Pacific El Niño event (x-axis) versus the mean longitude of the dynamic warm pool edge (y-axis) for a 60-year simulation (1948-2007) of the flux-forced ACCESS-OM model. This ACCESS-OM simulation does not have any El Niño events classified as double peaked using the definition in section 2.3.

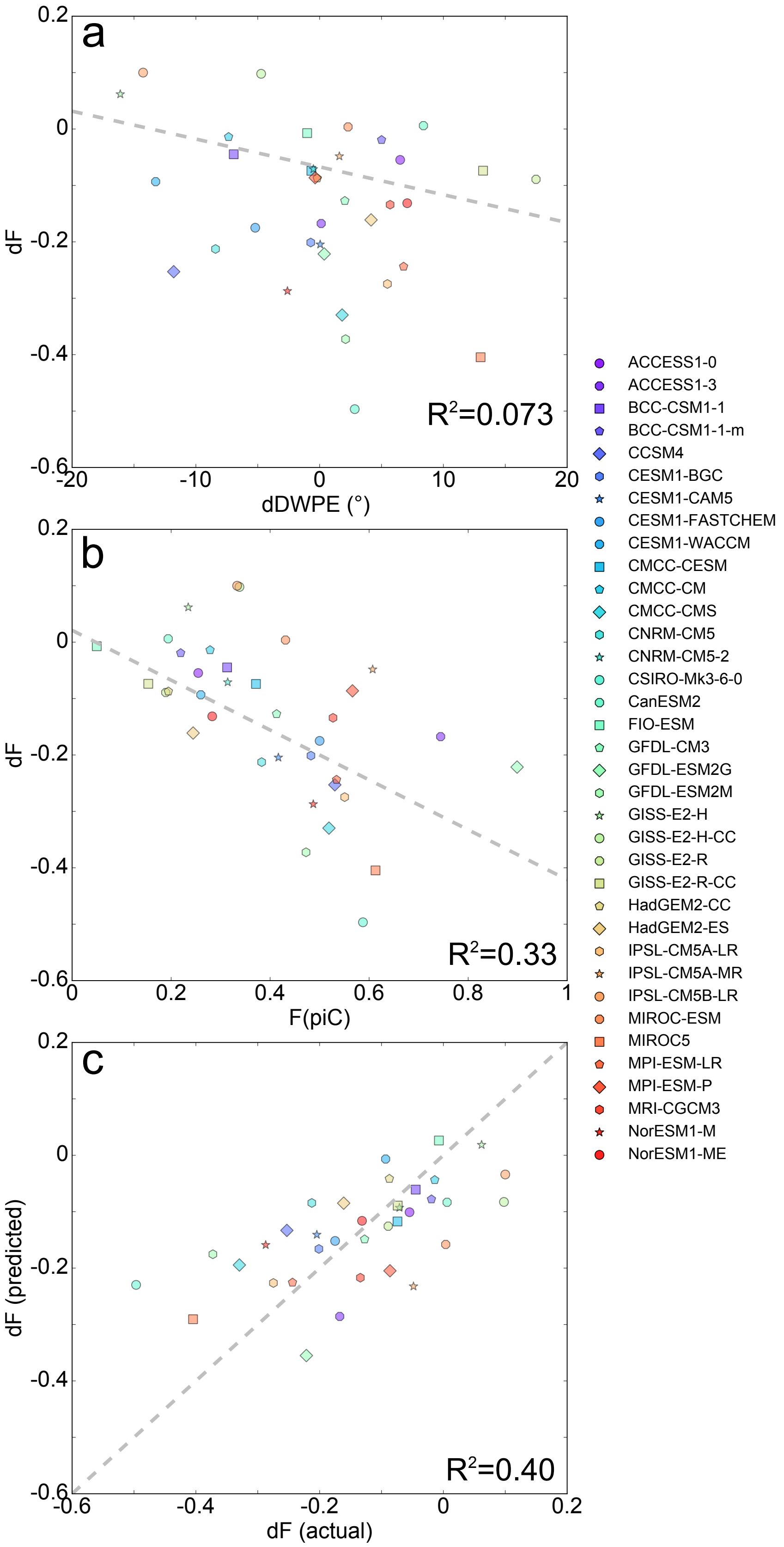

Fig. 6 The relationship between: **a** the change in the mean position of the dynamic warm pool edge (dDWPE) and the change in the fraction of double peaked El Niño events (dF) from the *historical* to the *PiControl* simulations; **b** the fraction of double peaked El Niño events in the *PiControl* simulations (F(piC) and the change in the fraction of double peaked El Niño events from the *historical* to the *PiControl* simulations; and **c** the actual and predicted (i.e., from equation (3)) change in the fraction of double peaked El Niño events from the *historical* to the *PiControl* simulations. The grey dashed lines in panels **a** and **b** represent the line of best fit from ordinary least squares regression, and in panel **c** represents the 1:1 line between the actual and predicted values. The R^2 values from the multiple linear regression analysis are reported.

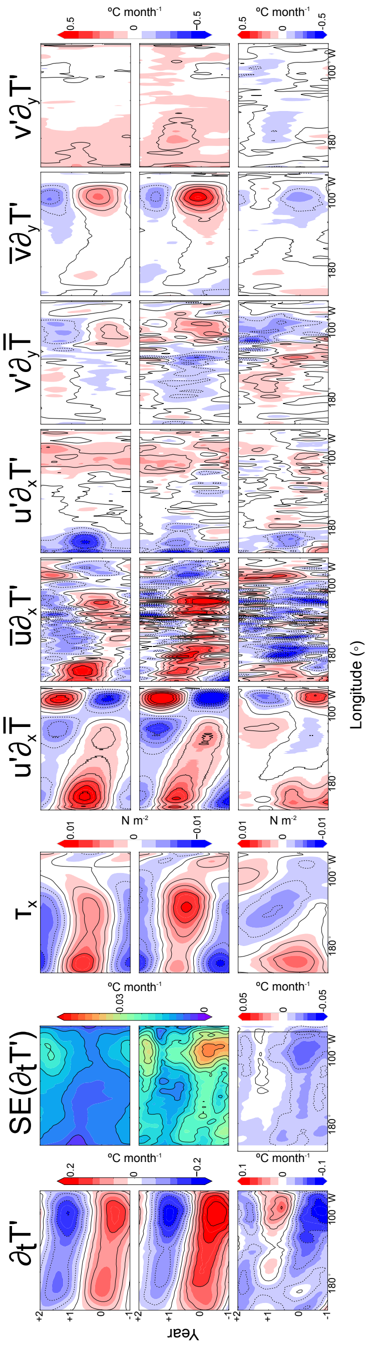

Fig. 7 Evolution of heat budget terms for the 36 months surrounding composite double peaked (top panels) El Niño events and eastern Pacific (middle panels) El Niño events from ACCESS-CM1.3. The bottom panels show the difference between the double peaked and eastern Pacific El Niño events. Data are averaged over 2°S-2°N. Wind stress anomaly (τ_x') data are in units of N m^{-2} (contour interval 0.01 N m^{-2}), and the units of the remaining panels are °C month^{-1} (contour interval 0.01°C month^{-01}). The interval between 0 and +1 represents the first year of the El Niño composite event. Note the difference in the color scale between the tendency term and the remaining heat budget feedbacks. The terms represented in each column are, from left: the mixed layer temperature tendency anomaly, the standard error (SE) of the mixed layer temperature tendency anomaly, the zonal wind stress anomaly, the zonal advective feedback ($-u'\partial_x\overline{T}$), the mean zonal advection term ($-\overline{u}\partial_x T'$), the anomalous zonal advection term, and the meridional heat budget terms.

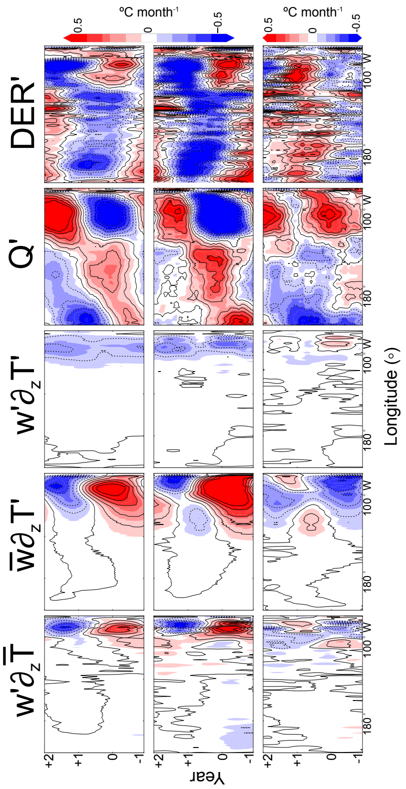

Fig. 7 (continued) As for previous figure, but this time, the terms represented in each column are, from left: the Ekman feedback ($-w'\partial_z\overline{T}$), the thermocline feedback ($-\overline{w}\partial_z T'$), the anomalous vertical advection term, the net surface heat flux anomaly (Q'), and the residual term *DER'*, namely, $\partial_t T' - (A'_x + A'_y + A'_z + Q')$.

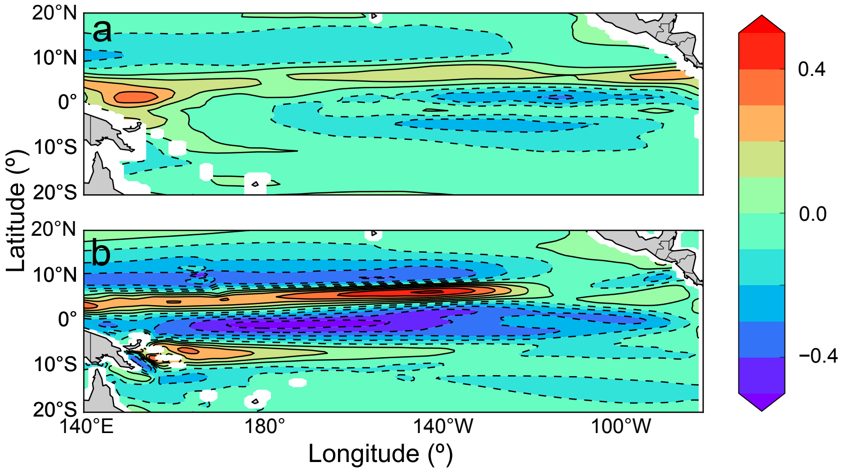

Fig. 8 Mean zonal currents over the period 1993-2005 (shading) derived from the **a** Ocean Surface Current Analyses Real-time (OSCAR; available at http://www.oscar.noaa.gov), and **b** the *historical* simulation of ACCESS-CM1.3. Data are in units of m s^{-1} and the contour interval is 0.1 m s^{-1}.

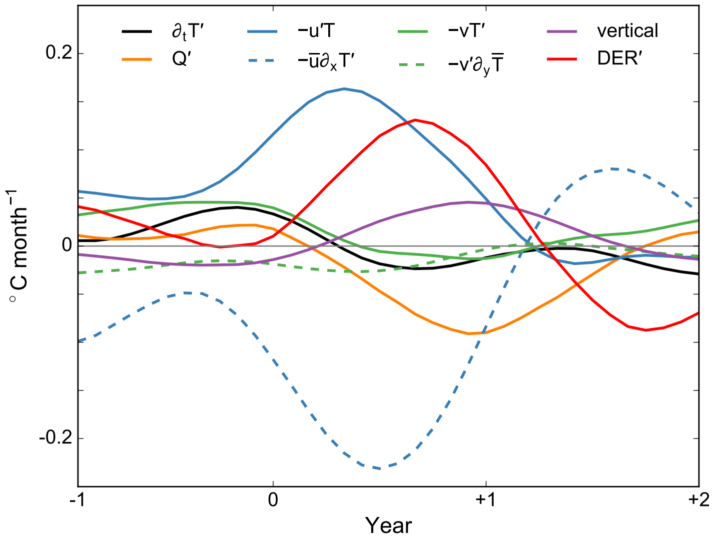

Fig. 9 Difference between ACCESS-CM1.3 heat budget terms (°C month^{-1}) in the central equatorial Pacific during double peaked and eastern Pacific El Niño events. Terms are calculated as the difference in the central equatorial Pacific at 154°W subtracted from the difference in the western-central equatorial Pacific at 178°E. The heat budget terms are as in figure 7, but with $-u'T = -u'\partial_x\overline{T} - u'\partial_x T'$, $-vT' = -v'\partial_y T' - \overline{v}\partial_y T'$, and vertical $= -\overline{w}\partial_z T' - w'\partial_z\overline{T} - w'\partial_z T'$.

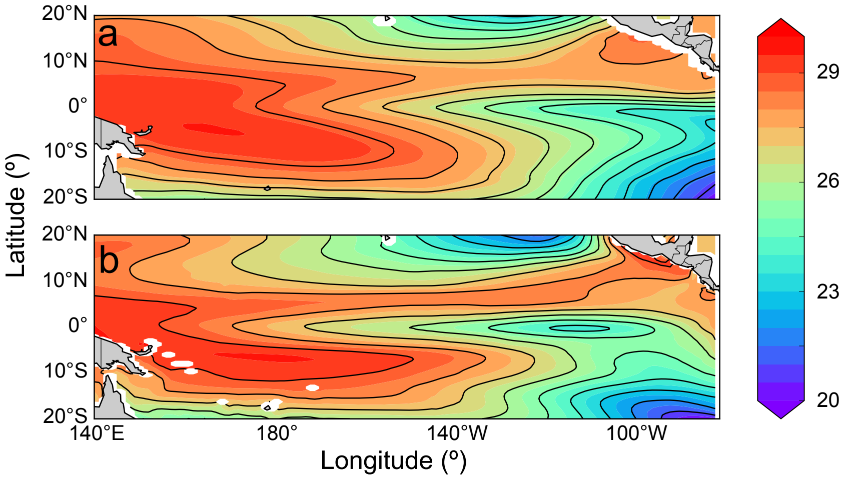

Fig. A1 Mean sea surface temperature over the period 1980-2004 (shading) in the **a** BMRC reanalyses, and **b** ACCESS-CM1.3. Data are in units of °C and the contour interval is 0.5°C.

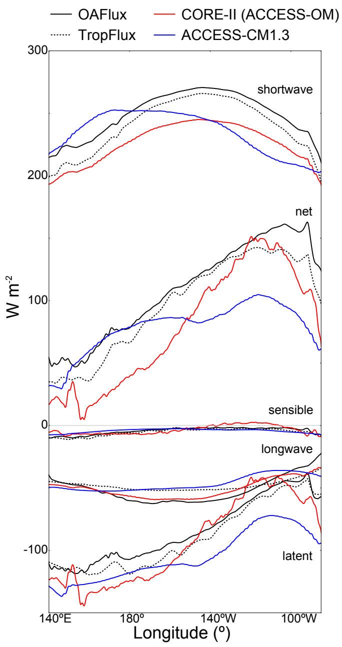

Fig. A2 Annual mean of equatorial surface heat flux variables - namely, shortwave, sensible, latent, longwave, and net heat fluxes - from ACCESS-CM1.3 (blue), the CORE-II reanalyses from ACCESS-OM (red), the OAFlux reanalyses (black solid), and the TropFlux reanalyses (black dashed). Data are averaged between 2°S and 2°N and are in units of W m^{-2}.

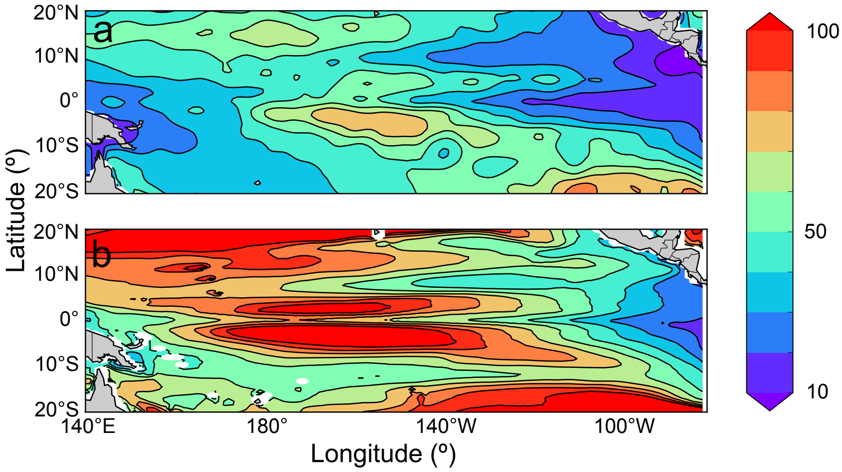

Fig. A3 Mean mixed layer depth (MLD) over the period 1980-2005 (shading) in the **a** UK Met Office (UKMO) reanalyses, and **b** ACCESS-CM1.3. The MLD is defined as the depth at which the density layer σ_t deviates from surface values by 0.125 kg m^{-3}. Contours show the bias in mean mixed layer depth with respect to the UKMO data. Data are in units of m and the contour interval is 10m.

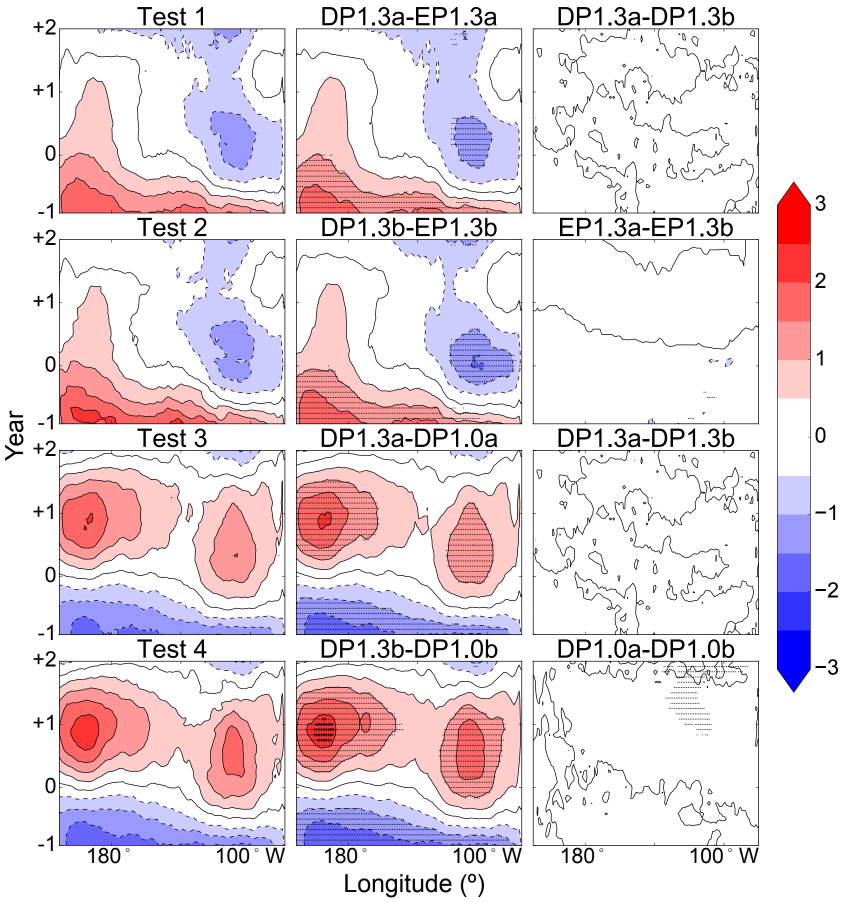

Fig. A4 Simple significance testing of SST' composites from randomly selected double peaked and eastern Pacific El Niño events in ACCESS-CM1.3 ($DP1.3a$, $DP1.3b$, $EP1.3a$, and $EP1.3b$, respectively) and double peaked El Niño events in in ACCESS-CM1.0 ($DP1.0a$, $DP1.0b$, respectively) for the 3 years surrounding El Niño events. Data displayed are median t probability density function values calculated from 100 random samples of the test groups a and b. The first column in each row is calculated by subtracting the third column from the second. Differences greater than one standard deviation from the mean are indicated with stippling ('.'), and differences significant at the 95% confidence interval with crosses ('+'). In each case, significance is calculated using a two-sided Student's t-test. The contour interval is 0.1.

Table 1: Summary of the El Niño spatial behaviors present in CMIP5 CGCMs based on the evolution of SST'. Unmarked data are sourced from *historical* simulations; Data marked with a $^+$ are derived from *PiControl* simulations.

Model		Reference	Years	El Niño events	DP events	DWPE isotherm	Mean longitude (σ) DWPE (°E)	Mean longitude (σ) western peak (°E)
ACCESS1-0	Australian Community Climate and Earth-System Simulator, version 1.0	Bi et al (2013a)	156	28	6	28.9	173 (9.2)	189 (7.3)
			500^+	106^+	27^+	28.2^+	167^+ (8.4^+)	184^+ (8.5^+)
ACCESS1-3	Australian Community Climate and Earth-System Simulator, version 1.3	Bi et al (2013a)	156	26	15	29.2	163 (9.1)	180 (6.3)
			500^+	89^+	65^+	28.7^+	163^+ (8.3^+)	176^+ (12.6^+)
BCC-CSM1-1	Beijing Climate Center, Climate System Model, version 1.1	Wu et al (2010)	163	37	11	28.2	164 (11.2)	191 (13.2)
			500^+	115^+	36^+	28.1^+	171^+ (9.8^+)	188^+ (15.4^+)
BCC-CSM1-1-M	Beijing Climate Center, Climate System Model, version 1.1 (medium resolution)	Wu et al (2010)	163	46	10	29.0	177 (13.5)	196 (11.6)
			400^+	114^+	47^+	28.9^+	172^+ (14.7^+)	182^+ (13.1^+)
CanESM2	Second Generation Canadian Earth System Model	Arora et al (2011);	156	36	8	28.6	176 (13.9)	175 (9.2)
		Gillett et al (2012)	996^+	268^+	52^+	27.7^+	168^+ (10.9^+)	174^+ (17.9^+)
CCSM4	Community Climate System Model, version 4	Gent et al (2011)	156	36	10	29.1	182 (14.7)	187 (18.7)
			1051^+	228^+	121^+	28.6^+	194^+ (11.6^+)	184^+ (14.2^+)
CESM1-BGC	Community Earth System Model	Long et al (2013)	156	29	9	29.1	185 (12.0)	191 (10.5)
			500^+	114^+	55^+	28.5^+	186^+ (15.9^+)	189^+ (8.1^+)
CESM1-CAM5	Community Earth System Model, version 1 (Community Earth System Model, version 5)	Meehl et al (2013)	156	33	7	28.4	175 (14.6)	187 (5.4)
			319^+	60^+	25^+	28.1^+	175^+ (13.7^+)	177^+ (9.0^+)
CESM1-FASTCHEM	Community Earth System Model, version 1, (with FASTCHEM)	Meehl et al (2013)	156	38	13	29.1	172 (12.2)	192 (9.8)
			222^+	48^+	24^+	29.1^+	177^+ (13.8^+)	196^+ (16.1^+)
CESM1-WACCM	Community Earth System Model, version 1 [with the Whole Atmosphere Community Climate Model (WACCM)]	Meehl et al (2013)	156	34	6	28.8	173 (14.7)	191 (9.1)
			200^+	50^+	13^+	28.6^+	186^+ (15.8^+)	197^+ (14.4^+)
CMCC-CESM	Centro Euro-Mediterraneo per I Cambiamenti Climatici Climate Model	Fogli et al (2009)	156	37	11	29.2	180 (14.0)	182 (10.1)
			277^+	70^+	26^+	28.3^+	181^+ (13.7^+)	186^+ (12.6^+)
CMCC-CM	Centro Euro-Mediterraneo per I Cambiamenti Climatici Climate Model	Fogli et al (2009)	156	30	9	28.9	172 (15.6)	192 (10.1)
			330^+	61^+	17^+	28.7^+	179^+ (17.5^+)	198^+ (19.1^+)
CMCC-CMS	Centro Euro-Mediterraneo per I Cambiamenti Climatici Climate Model	Fogli et al (2009)	156	37	7	28.4	181 (14.2)	194 (7.5)
			500^+	106^+	55^+	28.7^+	179^+ (10.9^+)	194^+ (12.0^+)
CNRM-CM5	Centre National de Recherches Mètèorologiques Coupled Global Climate Model, version 5	Voldoire et al (2013)	156	41	8	28.4	161 (11.6)	183 (23.2)
			850^+	222^+	85^+	28.5^+	170^+ (13.0^+)	186^+ (16.2^+)
CNRM-CM5-2	Centre National de Recherches Mètèorologiques Coupled Global Climate Model, version 5	Voldoire et al (2013)	156	36	9	28.2	164 (12.8)	187 (7.2)
			410^+	105^+	33^+	28.0^+	165^+ (13.5^+)	183^+ (16.0^+)
CSIRO-Mk3-6-0	Commonwealth Scientific and Industrial Research Organisation Mark, version 3.6.0	Rotstayn et al (2012)	156	29	3	27.8	155 (6.1)	189 (0.9)

			500^{+}	80^{+}	47^{+}	27.0^{+}	152^{+} (5.3^{+})	193^{+} (10.8^{+})
FIO-ESM	First Institute of Oceanography Earth System Model	Qiao et al (2013)	156	45	2	28.9	179 (19.7)	204 (12.4)
			800^{+}	241^{+}	12^{+}	29.2^{+}	180^{+} (19.7^{+})	195^{+} (16.9^{+})
GFDL-CM3	Geophysical Fluid Dynamics Laboratory Climate Model, version 3	Donner et al (2011);	146	40	12	28.7	166 (13.2)	167 (18.9)
		Griffies et al (2011)	800^{+}	184^{+}	76^{+}	28.4^{+}	164^{+} (10.8^{+})	169^{+} (20.7^{+})
GFDL-ESM2G	Geophysical Fluid Dynamics Laboratory Earth System Model with Generalized Ocean Layer Dynamics (GOLD) component	Dunne et al (2012)	145	27	21	28.3	156 (6.6)	159 (18.3)
			500^{+}	89^{+}	80^{+}	28.2^{+}	156^{+} (7.7^{+})	156^{+} (19.1^{+})
GFDL-ESM2M	Geophysical Fluid Dynamics Laboratory Earth System Model with Modular Ocean Model 4 (MOM4) component	Dunne et al (2012)	145	30	3	28.6	174 (19.3)	166 (19.1)
			500^{+}	91^{+}	43^{+}	28.8^{+}	172^{+} (15.8^{+})	176^{+} (8.0^{+})
GISS-E2-H	Goddard Institute for Space Studies Model E2, coupled with the Hybrid Coordinate Ocean Model (HYCOM)	Miller (2014);	156	24	8	28.4	167 (14.0)	176 (28.9)
		Schmidt et al (2014)	1770^{+}	162^{+}	38^{+}	28.9^{+}	183^{+} (19.4^{+})	186^{+} (18.2^{+})
GISS-E2-H-CC	Goddard Institute for Space Studies Model E2, coupled with the Hybrid Coordinate Ocean Model (HYCOM) and Carbon Cycle	Miller (2014);	161	37	17	28.4	173 (17.1)	194 (26.6)
		Schmidt et al (2014)	251^{+}	71^{+}	24^{+}	28.9^{+}	178^{+} (18.7^{+})	194^{+} (22.5^{+})
GISS-E2-R	Goddard Institute for Space Studies Model E2, coupled with the Russell ocean model	Miller (2014);	156	28	3	28.9	191 (17.9)	214 (16.4)
		Schmidt et al (2014)	1200^{+}	148^{+}	28^{+}	28.7^{+}	174^{+} (16.1^{+})	199^{+} (9.8^{+})
GISS-E2-R-CC	Goddard Institute for Space Studies Model E2, coupled with the Russell ocean model and Carbon Cycle	Miller (2014);	161	24	2	28.9	188 (18.7)	184 (8.8)
		Schmidt et al (2014)	251^{+}	39^{+}	6^{+}	28.8^{+}	175^{+} (16.4^{+})	194^{+} (11.5^{+})
HadGEM2-CC	Hadley Centre Global Environment Model, version 2 - Carbon Cycle	Collins et al (2011);	146	28	3	27.9	171 (8.9)	206 (8.1)
		Martin et al (2011)	240^{+}	36^{+}	7^{+}	27.7^{+}	171^{+} (8.5^{+})	179^{+} (0.0^{+})
HadGEM2-ES	Hadley Centre Global Environment Model, version 2 - Earth System	Collins et al (2011);	146	24	2	28.2	167 (9.0)	190 (4.5)
		Martin et al (2011)	576^{+}	90^{+}	22^{+}	28.0^{+}	163^{+} (8.6^{+})	224^{+} (7.0^{+})
IPSL-CM5A-LR	L'Institut Pierre-Simon Laplace Coupled Model, version 5A coupled with NEMO low resolution	Dufresne et al (2013)	156	28	8	28.3	157 (7.2)	162 (24.9)
			1000^{+}	178^{+}	98^{+}	28.3^{+}	151^{+} (6.0^{+})	162^{+} (19.1^{+})
IPSL-CM5A-MR	L'Institut Pierre-Simon Laplace Coupled Model, version 5A coupled with NEMO medium resolution	Dufresne et al (2013)	156	31	19	29.2	158 (9.1)	174 (18.5)
			300^{+}	56^{+}	34^{+}	29.0^{+}	157^{+} (8.6^{+})	162^{+} (20.7^{+})
IPSL-CM5B-LR	L'Institut Pierre-Simon Laplace Coupled Model, version 5B, coupled with NEMO low resolution	Dufresne et al (2013)	156	29	13	28.7	167 (12.3)	190 (18.7)
			300^{+}	63^{+}	21^{+}	28.7^{+}	181^{+} (12.1^{+})	190^{+} (11.9^{+})
MIROC-ESM	Model for Interdisciplinary Research on Climate, Earth System Model	Watanabe et al (2011)	156	17	10	27.7	155 (6.3)	157 (13.0)
			680^{+}	58^{+}	25^{+}	27.9^{+}	152^{+} (5.6^{+})	154^{+} (15.8^{+})
MIROC5	Model for Interdisciplinary Research on Climate, version 5	Watanabe et al (2010)	163	23	5	28.5	174 (18.8)	158 (15.1)
			670^{+}	93^{+}	57^{+}	28.2^{+}	161^{+} (12.1^{+})	171^{+} (11.5^{+})
MPI-ESM-LR	Max Planck Institute Earth System Model, low resolution	Giorgetta et al (2013)	156	27	9	28.4	166 (15.2)	162 (12.4)

			1000^+	161^+	86^+	28.6^+	159^+ (7.3^+)	162^+ (21.1^+)
MPI-ESM-P	Max Planck Institute Earth System Model	Giorgetta et al (2013)	156	23	12	28.9	161 (8.9)	162 (25.0)
			1156^+	196^+	111^+	28.7^+	161^+ (10.3^+)	162^+ (20.3^+)
MRI-CGCM3	Meteorological Research Institute Coupled Atmosphere-Ocean General Circulation Model, version 3	Yukimoto et al (2012)	156	28	11	28.2	170 (8.4)	194 (20.1)
			500^+	74^+	39^+	28.1^+	164^+ (7.2^+)	181^+ (9.9^+)
NorESM1-M	Norwegian Earth System Model, version 1 (intermediate resolution)	Bentsen et al (2013)	156	42	9	28.4	166 (11.3)	180 (18.5)
			501^+	117^+	57^+	28.7^+	169^+ (12.8^+)	187^+ (8.4^+)
NorESM1-ME	Norwegian Earth System Model, version 1 (intermediate resolution) with interactive carbon cycle	Bentsen et al (2013)	156	30	5	28.4	176 (12.0)	178 (13.1)
			252^+	53^+	15^+	28.2^+	169^+ (12.1^+)	192^+ (7.6^+)

Table 2 Fitted values and confidence intervals for the parameters in equation (3).

Parameter	Estimate	95% confidence interval	
		Min	Max
a	-0.0049	-0.010	0
b	-0.44	-0.65	-0.23
c	0.043	-0.049	0.14

References

AchutaRao K, Sperber KR (2006) ENSO simulation in coupled ocean-atmosphere models: are the current models better? Climate Dynamics 27:1–15, DOI 10.1007/s00382-006-0119-7

Allan R (2000) El Niño and the Southern Oscillation: multiscale variability, global and regional impacts, Cambridge University Press, UK, p 356

Allan RJ, Reason CJC, Lindesay JA, Ansell TJ (2003) Protracted ENSO episodes and their impacts in the Indian Ocean region. Deep Sea Research II: Topical Studies in Oceanography 50(12-13):2331–2347, DOI 10.1016/S0967-0645(03)00059-6

Arora VK, Scinocca JF, Boer GJ, Christian JR, Denman KL, Flato GM, Kharin VV, Lee WG, Merryfield WJ (2011) Carbon emission limits required to satisfy future representative concentration pathways of greenhouse gases. Geophysical Research Letters 38(5):3–8, DOI 10.1029/2010GL046270

Ashok K, Behera SK, Rao SA, Weng H, Yamagata T (2007) El Niño Modoki and its possible teleconnection. Journal of Geophysical Research 112(C11):1–27, DOI 10.1029/2006JC003798

Bellenger H, Guilyardi E, Leloup J, Lengaigne M, Vialard J (2014) ENSO representation in climate models: from CMIP3 to CMIP5. Climate Dynamics 42(7-8):1999–2018, DOI 10.1007/s00382-013-1783-z

Belmadani A, Dewitte B, An SI (2010) ENSO feedbacks and associated time scales of variability in a multimodel ensemble. Journal of Climate 23(12):3181–3204, DOI 10.1175/2010JCLI2830.1

Bentsen M, Bethke I, Debernard JB, Iversen T, Kirkevåg A, Seland Ø, Drange H, Roelandt C, Seierstad IA, Hoose C, Kristjánsson JE (2013) The Norwegian Earth System Model, NorESM1-M – part 1: Description and basic evaluation of the physical climate. Geoscientific Model Development 6(3):687–720, DOI 10.5194/GMD-6-687-2013

Bi D, Dix M, Marsland SJ, O'Farrell S, Rashid HA, Uotila P, Hirst AC, Kowalczyk E, Golebiewski M, Sullivan A, Yan H, Hannah N, Franklin C, Sun Z, Vohralik P, Watterson I, Zhou X, Fiedler R, Collier M, Ma Y, Noonan J, Stevens L, Uhe P, Zhu H, Griffies SM, Hill R, Harris C, Puri K (2013a) The ACCESS coupled model: description, control climate and evaluation. Australian Meteorological and Oceanographic Journal 63:41–64

Bi D, Marsland SJ, Uotila P, O'Farrell S, Fiedler R, Sullivan A, Griffies SM, Zhou X, Hirst AC (2013b) ACCESS-OM: the ocean and sea-ice core of the ACCESS coupled model. Australian Meteorological and Oceanographic Journal 63:213–232

Boucharel J, Dewitte B, du Penhoat Y, Garel B, Yeh SW, Kug JS (2011) ENSO nonlinearity in a warming climate. Climate Dynamics 37:2045–2065, DOI 10.1007/s00382-011-1119-9

Brown JN, Langlais C, Maes C (2013) Zonal structure and variability of the western Pacific dynamic warm pool edge in CMIP5. Climate Dynamics 42(11-12):3061–3076, DOI 10.1007/s00382-013-1931-5

Capotondi A (2013) ENSO diversity in the NCAR CCSM4 climate model. Journal of Geophysical Research 118:1–16, DOI 10.1002/jgrc.20335

Capotondi A, Wittenberg AT, Masina S (2006) Spatial and temporal structure of tropical Pacific interannual variability in 20th century coupled simulations. Ocean Modelling 15:274–298, DOI 10.1016/j.ocemod.2006.02.004

Capotondi A, Ham YG, Wittenberg AT, Kug JS (2015a) Climate model biases and El Niño Southern Oscillation (ENSO) simulation. US CLIVAR variations 13(1):21–25

Capotondi A, Wittenberg AT, Newman M, Di Lorenzo E, Yu JY, Braconnot P, Cole J, Dewitte B, Giese BS, Guilyardi E, Jin FF, Karnauskas KB, Kirtman BP, Lee T, Schneider N, Xue Y, Yeh SW (2015b) Understanding ENSO diversity. Bulletin of the American Meteorological Society DOI 10.1175/BAMS-D-13-00117.1

Choi J, An SI, Yeh SW (2012) Decadal amplitude modulation of two types of ENSO and its relationship with the mean state. Climate Dynamics 38(11-12):2631–2644, DOI 10.1007/s00382-011-1186-y
Choi K, Vecchi GA, Wittenberg AT (2013) ENSO transition, duration and amplitude asymmetries: role of the nonlinear wind stress coupling in a conceptual model. Journal of Climate 26:9462–9476, DOI 10.1175/JCLI-D-13-00045.1
Choi KY, Vecchi GA, Wittenberg AT (2015) Nonlinear zonal wind response to ENSO in the CMIP5 models: roles of the zonal and meridional shift of the ITCZ/SPCZ and the simulated climatological precipitation. Journal of Climate 28:8556–8573, DOI 10.1175/JCLI-D-15-0211.1
Clarke AJ, Wang J, Van Gorder S (2000) A simple warm-pool displacement ENSO model. Journal of Physical Oceanography 30:1679–1691
Collins M, An SI, Ganachaud A, Guilyardi E, Jin FF, Jochum M, Lengaigne M, Power S, Timmermann A, Vecchi GA, Wittenberg AT (2010) The impact of global warming on the tropical Pacific Ocean and El Niño. Nature Geoscience 3:391–367, DOI 10.1038/NGEO868
Collins WJ, Bellouin N, Doutriaux-Boucher M, Gedney N, Halloran P, Hinton T, Hughes J, Jones CD, Joshi M, Liddicoat S, Martin G, O'Connor F, Rae J, Senior C, Sitch S, Totterdell I, Wiltshire a, Woodward S (2011) Development and evaluation of an Earth-System model – HadGEM2. Geoscientific Model Development 4:1051–1075, DOI 10.5194/gmd-4-1051-2011
Deser C, Phillips AS, Tomas RA, Okumura YM, Alexander MA, Capotondi A, Scott JD, Kwon YO, Ohba M (2012) ENSO and Pacific decadal variability in the Community Climate System Model Version 4. Journal of Climate 25:2622–2651, DOI 10.1175/JCLI-D-11-00301.1
DiNezio PN, Kirtman BP, Clement AC, Lee SK, Vecchi GA, Wittenberg AT (2012) Mean climate controls on the simulated response of ENSO to increasing greenhouse gases. Journal of Climate 24:7399–7420, DOI 10.1175/JCLI-D-11-00494.1
Dix M, Vohralik P, Bi D, Rashid H, Marsland S, OFarrell S, Uotila P, Hirst T, Kowalczyk E, Sullivan A, Yan H, Franklin C, Sun Z, Watterson I, Collier M, Noonan J, Stevens L, Uhe P, Puri K (2014) The ACCESS coupled model: Documentation of core CMIP5 simulations and initial results. Australian Meteorological and Oceanographic Journal 63:83–99
Donner LJ, Wyman BL, Hemler RS, Horowitz LW, Ming Y, Zhao M, Golaz JC, Ginoux P, Lin SJ, Schwarzkopf MD, Austin J, Alaka G, Cooke WF, Delworth TL, Freidenreich SM, Gordon CT, Griffies SM, Held IM, Hurlin WJ, Klein Sa, Knutson TR, Langenhorst AR, Lee HC, Lin Y, Magi BI, Malyshev SL, Milly PCD, Naik V, Nath MJ, Pincus R, Ploshay JJ, Ramaswamy V, Seman CJ, Shevliakova E, Sirutis JJ, Stern WF, Stouffer RJ, Wilson RJ, Winton M, Wittenberg AT, Zeng F (2011) The dynamical core, physical parameterizations, and basic simulation characteristics of the atmospheric component AM3 of the GFDL global coupled model CM3. Journal of Climate 24(13):3484–3519, DOI 10.1175/2011JCLI3955.1
Dufresne JL, Foujols MA, Denvil S, Caubel A, Marti O, Aumont O, Balkanski Y, Bekki S, Bellenger H, Benshila R, Bony S, Bopp L, Braconnot P, Brockmann P, Cadule P, Cheruy F, Codron F, Cozic A, Cugnet D, de Noblet N, Duvel JP, Ethé C, Fairhead L, Fichefet T, Flavoni S, Friedlingstein P, Grandpeix JY, Guez L, Guilyardi E, Hauglustaine D, Hourdin F, Idelkadi A, Ghattas J, Joussaume S, Kageyama M, Krinner G, Labetoulle S, Lahellec A, Lefebvre MP, Lefevre F, Levy C, Li ZX, Lloyd J, Lott F, Madec G, Mancip M, Marchand M, Masson S, Meurdesoif Y, Mignot J, Musat I, Parouty S, Polcher J, Rio C, Schulz M, Swingedouw D, Szopa S, Talandier C, Terray P, Viovy N, Vuichard N (2013) Climate change projections using the IPSL-CM5 Earth System Model: From CMIP3 to CMIP5. Climate Dynamics 40(9-10):2123–2165, DOI 10.1007/s00382-012-1636-1
Dunne JP, John JG, Adcroft AJ, Griffies SM, Hallberg RW, Shevliakova E, Stouffer RJ, Cooke W, Dunne KA, Harrison MJ, Krasting JP, Malyshev SL, Milly PCD, Phillipps PJ, Sentman LT, Samuels BL, Spelman MJ, Winton M, Wittenberg AT, Zadeh N (2012) GFDL's ESM2 global

coupled climate–carbon earth system models. Part I: Physical formulation and baseline simulation characteristics. Journal of Climate 25(19):6646–6665, DOI 10.1175/JCLI-D-11-00560.1
Fogli PG, Manzini E, Vichi M, Alessandri A, Patara L, Gualdi S, Scoccimarro E, Masina S, Navarra A (2009) INGV - CMCC Carbon (ICC): A carbon cycle earth system model. Tech. Rep. April, Centro Euro-Mediterraneo Per I Cambiamenti Climatici
Gebbie G, Eisenman I, Wittenberg AT, Tziperman E (2007) Modulation of westerly wind bursts by sea surface temperature: A semistochastic feedback for ENSO. Journal of the Atmospheric Sciences 64:3281–3295, DOI 10.1175/JAS4029.1
Gent PR, Danabasoglu G, Donner LJ, Holland MM, Hunke EC, Jayne SR, Lawrence DM, Neale RB, Rasch PJ, Vertenstein M, Worley PH, Yang ZL, Zhang M (2011) The community climate system model version 4. Journal of Climate 24(19):4973–4991, DOI 10.1175/2011JCLI4083.1
Giese BS, Ray S (2011) El Niño variability in simple ocean data assimilation (SODA). Journal of Geophysical Research 116, DOI 10.1029/2010JC006695
Gillett NP, Arora VK, Flato GM, Scinocca JF, Von Salzen K (2012) Improved constraints on 21st-century warming derived using 160 years of temperature observations. Geophysical Research Letters 39(1):1–5, DOI 10.1029/2011GL050226
Giorgetta MA, Jungclaus J, Reick CH, Legutke S, Bader J, Böttinger M, Brovkin V, Crueger T, Esch M, Fieg K, Glushak K, Gayler V, Haak H, Hollweg HD, Ilyina T, Kinne S, Kornblueh L, Matei D, Mauritsen T, Mikolajewicz U, Mueller W, Notz D, Pithan F, Raddatz T, Rast S, Redler R, Roeckner E, Schmidt H, Schnur R, Segschneider J, Six KD, Stockhause M, Timmreck C, Wegner J, Widmann H, Wieners KH, Claussen M, Marotzke J, Stevens B (2013) Climate and carbon cycle changes from 1850 to 2100 in MPI-ESM simulations for the Coupled Model Intercomparison Project phase 5. Journal of Advances in Modeling Earth Systems 5(3):572–597, DOI 10.1002/jame.20038
Graham FS, Brown JN, Langlais C, Marsland SJ, Wittenberg AT, Holbrook NJ (2014) Effectiveness of the Bjerknes stability index in representing ocean dynamics. Climate Dynamics DOI 10.1007/s00382-014-2062-3
Graham FS, Brown JN, Wittenberg AT, Holbrook NJ (2015) Reassessing conceptual models of ENSO. Journal of Climate 28:9121–9142, DOI 10.1175/JCLI-D-14-00812.1
Griffies SM (2009) Elements of MOM4p1: GFDL Ocean Group. Tech. Rep. 6, NOAA Geophysical Fluid Dynamics Laboratory
Griffies SM, Winton M, Donner LJ, Horowitz LW, M DS, Farneti R, Gnanadesikan A, Hurlin WJ, Lee HC, Palter JB, Samuels BL, Wittenberg AT, Wyman B, Yin J, Zadeh N (2011) The GFDL CM3 coupled climate model: characteristics of the ocean and sea ice simulations. Journal of Climate 24(13):3520–3544, DOI 10.1175/2077JCLI3964.1
Griffies SM, Winton M, Samuels BL, Danabasoglu G, Yeager SG, Marsland SJ, Drange H, Bentsen M (2012) Datasets and Protocol for the CLIVAR WGOMD Coordinated Ocean-Sea Ice Reference Experiments (COREs). WCRP Report No. 21/2012, pp. 21
Guilyardi E, Wittenberg AT, Fedorov AV, Collins M, Wang C, Capotondi A, van Oldenborgh GJ, Stockdale T (2009) Understanding El Niño in ocean-atmosphere general circulation models. Bulletin of the American Meteorological Society 90:325–340, DOI 10.1175/2008BAMS2387.1
Guilyardi E, Cai W, Collins M, Fedorov AV, Jin FF, Kumar A, Sun DZ, Wittenberg AT (2012) New strategies for evaluating ENSO processes in climate models. Bulletin of the American Meteorological Society 93:235–238, DOI 10.1175/BAMS-D-11-00106.1
Guilyardi E, Bellenger H, Collins M, Ferrett S, Cai W, Wittenberg AT (2013) A first look at ENSO in CMIP5. Clivar Exchanges 17(1):29–32
Guilyardi E, Wittenberg AT, Balmaseda M, Cai W, Collins M, McPhaden MJ, Watanabe M, Yeh SW (2015) ENSO in a changing climate - meeting summary of the 4th CLIVAR workshop on the evaluation of ENSO processes in climate models. Bulletin of the American Meteorological

Society DOI 10.1175/BAMS-D-15-00287.1, in press
Ham YG, Kug JS (2012) How well do current climate models simulate two types of El Niño? Climate Dynamics 39:383–398, DOI 10.1007/s00382-011-1157-3
Holbrook NJ, Li J, Collins M, Di Lorenzo E, Jin FF, Knutson TR, Latif M, Li C, Power SB, Huang R, Wu G (2014) Decadal climate variability and cross-scale interactions: ICCL 2013 Expert Assessment Workshop. Bulletin of the American Meteorological Society 95(ES155-ES158), DOI 10.1175/BAMS-D-13-00201.1
Huang BH, Xue Y, Zhang D, Kumar A, McPhaden MJ (2010) The NCEP GODAS ocean analysis of the tropical Pacific mixed layer heat budget on seasonal to interannual timescales. Journal of Climate 23:4901–4925
Huang BH, Xue Y, Wang H, Wang W, Kumar A (2011) Mixed layer heat budget of the El Niño in NCEP climate forecast system. Climate Dynamics DOI 10.1007/s00382-011-1111-4
Ingleby B, Huddleston M (2007) Quality control of ocean temperature and salinity profiles - historical and real-time data. Journal of Marine Systems 65:158–175, DOI 10.1016/j.jmarsys.2005.11.019
Jia L, Yang X, Vecchi GA, Gudgel RG, Delworth TL, Rosati A, Stern WF, Wittenberg AT, Krishnamurthy L, Zhang S, Msadek R, Kapnick S, Underwood SD, Zeng F, Anderson WG, Balaji V, Dixon KW (2015) Improved seasonal prediction of temperature and precipitation over land in a high-resolution GFDL climate model. Journal of Climate 28:2044–2062, DOI 10.1175/JCLI-D-14-00112.1
Jin FF (1997a) An equatorial ocean recharge paradigm for ENSO. Part I: Conceptual model. Journal of the Atmospheric Sciences 54:811–829
Jin FF (1997b) An equatorial ocean recharge paradigm for ENSO. Part II: A stripped-down coupled model. Journal of the Atmospheric Sciences 54:830–847
Johnson NC (2013) How many ENSO flavors can we distinguish? Journal of Climate 26(13):4816–4827, DOI 10.1175/JCLI-D-12-00649.1
Kalnay E, Kanamitsu M, Kistler R, Collins W, Deaven D, Gandin L, Iredell M, Saha S, White G, Woollen J, Zhu Y, Leetmaa A, Reynolds R, Chelliah M, Ebisuzaki W, Higgins W, Janowiak J, Mo KC, Ropelewski C, Wang J, Jenne R, Joseph D (1996) The NCEP/NCAR 40-year reanalysis project. Bulletin of the American Meteorological Society 77:437–471
Kao HY, Yu JY (2009) Contrasting eastern-Pacific and central-Pacific types of ENSO. Journal of Climate 22(3):615–632, DOI 10.1175/2008JCLI2309.1
Kim ST, Jin FF (2011) An ENSO stability analysis. Part II: results from the twentieth and twenty-first century simulations of the CMIP3 models. Climate Dynamics 36:1609–1627, DOI 10.1007/s00382-010-0872-5
Kim ST, Cai W, Jin FF, Yu JY (2014) ENSO stability in coupled climate models and its association with mean state. Climate Dynamics 42(11-12):3313–3321, DOI 10.1007/s00382-013-1833-6
Krishnamurthy L, Vecchi GA, Msadek R, Wittenberg AT, Delworth TL, Zeng F (2015) The seasonality of the Great Plains Low-Level Jet and ENSO relationship. Journal of Climate 28:4825–4544, DOI 10.1175/JCLI-D-14-00590.1
Krishnamurthy L, Vecchi GA, Msadek R, Murakami H, Wittenberg AT, Zeng F (2016) Impact of strong ENSO on regional tropical cyclone activity in a high-resolution climate model in the North Pacific and North Atlantic. Journal of Climate 29:2375–2394, DOI 10.1175/JCLI-D-0468.1
Kug JS, Choi J, An SI, Jin FF, Wittenberg AT (2010) Warm pool and cold tongue El Niño events as simulated by the GFDL 2.1 coupled GCM. Journal of Climate 23:1226–1239, DOI 10.1175/2009JCLI3293.1
Kumar BP, Vialard J, Lengaigne M, Murty VSN, McPhaden MJ (2012) TropFlux: air-sea fluxes for the global tropical oceans - description and evaluation. Climate Dynamics 38(7-8):1521–

1543
Latif M, Semenov VA, Park W (2015) Super El Niños in response to global warming in a climate model. Climate Dynamics 132:489–500, DOI 10.1007/s10584-015-1439-6
Lee SK, DiNezio PN, Chung ES, Yeh SW, Wittenberg AT, Wang C (2014) Spring persistence, transition and resurgence of El Niño. Geophysical Research Letters 41(23):8578–8585, DOI 10.1002/2014GL062484
Lee T, McPhaden MJ (2010) Increasing intensity of El Niño in the central-equatorial Pacific. Geophysical Research Letters 37:L14,603, DOI 10.1029/2010GL0440007
Leloup J, Lengaigne M, Boulanger JP (2008) Twentieth century ENSO characteristics in the IPCC database. Climate Dynamics 30:277–291
Lloyd J, Guilyardi E, Weller H, Slingo J (2009) The role of atmosphere feedbacks during ENSO in the CMIP3 models. Atmospheric Science Letters 10:170–176
Lloyd J, Guilyardi E, Weller H (2012) The role of atmosphere feedbacks during ENSO in the CMIP3 models. Part III: the shortwave flux feedback. Journal of Climate 25(12):4275–4293, DOI 10.1175/JCLI-D-11-00178.1
Long MC, Lindsay K, Peacock S, Moore JK, Doney SC (2013) Twentieth-century oceanic carbon uptake and storage in CESM1(BGC). Journal of Climate 26(18):6775–6800, DOI 10.1175/JCLI-D-12-00184.s1
Martin GM, Bellouin N, Collins WJ, Culverweil ID, Halloran P, Hardiman S, Hinton TJ, Jones CD, McLaren A, O'Connor F, Rodriguez J, Woodward S, et al (2011) The HadGEM2 family of Met Office Unified Model climate configurations. Geoscientific Model Development Discussions 4:723–757, DOI 10.5194/gmd-4-723-2011
Meehl GA, Teng H, Branstator G (2006) Future changes of El Niño in two coupled climate models. Climate Dynamics 26(6):549–566, DOI 10.1007/s00382-005-0098-0
Meehl GA, Washington WM, Arblaster JM, Hu A, Teng H, Kay JE, Gettelman A, Lawrence DM, Sanderson BM, Strand WG (2013) Climate change projections in CESM1(CAM5) compared to CCSM4. Journal of Climate 26(17):6287–6308, DOI 10.1175/JCLI-D-12-00572.1
Miller RL (2014) CMIP5 historical simulations (1850–2012) with GISSModelE2. Journal of Advances in Modeling Earth Systems pp 441–477, DOI 10.1002/2013MS000266.Received
Ogata T, Xie SP, Wittenberg AT, Sun DZ (2013) Interdecadal amplitude modulation of El Niño/Southern Oscillation and its impacts on tropical Pacific decadal variability. Journal of Climate 26:7280–7297, DOI 10.1175/JCLI-D-12-00415.1
Picaut J, Ioualalen M, Menkes C, Delcroix T, McPhaden MJ (1996) Mechanism of the zonal displacements of the Pacific warm pool: Implications for ENSO. Science (New York, NY) 274(5292):1486–9
Picaut J, Masia F, du Penhoat Y (1997) An advective-reflective conceptual model for the oscillatory nature of the ENSO. Science 277(5326):663–666, DOI 10.1126/science.277.5326.663
Qiao F, Song Z, Bao Y, Song Y, Shu Q, Huang C, Zhao W (2013) Development and evaluation of an Earth System Model with surface gravity waves. Journal of Geophysical Research: Oceans 118(9):4514–4524, DOI 10.1002/jgrc.20327
Rashid HA, Hirst AC (2015) Investigating the mechanisms of seasonal ENSO phase locking bias in the ACCESS coupled model. Climate Dynamics DOI 10.1007/s00382-015-2633-y
Rashid HA, Hirst AC, Dix M (2013a) Atmospheric circulation features in the ACCESS model simulations for CMIP5: historical simulation and future projections. Australian Meteorological and Oceanographic Journal 63:145–160
Rashid HA, Sullivan A, Hirst AC, Bi D, Marsland SJ (2013b) Evaluation of El Niño-Southern Oscillation in the ACCESS coupled model simulations for CMIP5. Australian Meteorological and Oceanographic Journal 63(1):161–180

Rasmusson EM, Carpenter TH (1982) Variations in tropical sea surface temperature and surface wind fields associated with the Southern Oscillation/El Niño. Monthly Weather Review 110:354–384

Rotstayn LD, Jeffrey SJ, Collier Ma, Dravitzki SM, Hirst aC, Syktus JI, Wong KK (2012) Aerosol- and greenhouse gas-induced changes in summer rainfall and circulation in the Australasian region: A study using single-forcing climate simulations. Atmospheric Chemistry and Physics 12(14):6377–6404, DOI 10.5194/acp-12-6377-2012

Schmidt GA, Kelley M, Nazarenko L, Ruedy R, Russell GL, Aleinov I, Bauer M, Bauer SE, Bhat MK, Bleck R, Canuto V, Chen Yh, Cheng Y, Clune TL, Genio AD, Fainchtein RD, Faluvegi G, Hansen JE, Healy RJ, Kiang NY, Koch D, Lacis AA, Legrande AN, Lerner J, Lo KK, Matthews EE, Menon S, Miller RL, Oinas V, Oloso AO (2014) Configuration and assessment of the GISS ModelE2 contributions to the CMIP5 archive. Journal of Advances in Modeling Earth Systems 6:141–184, DOI 10.1002/2013MS000265

Smith NR (1995) An improved system for tropical ocean subsurface temperature analyses. Journal of Atmospheric and Oceanic Technology 12:850–870

Taschetto AS, Sen Gupta A, Jourdain NC, Santoso A, Ummenhofer CC, England MH (2014) Cold Tongue and Warm Pool ENSO events in CMIP5: mean state and future projections. Journal of Climate 27:2861–2885, DOI 10.1175/JCLI-D-13-00437.1

Taylor KE, Stouffer RJ, Meehl GA (2012) Overview of CMIP5 and the experiment design. Bulletin of the American Meteorological Society 93:485–498, DOI http://dx.doi.org/10.1175/BAMS-D-11-00094.1

Trenberth KE (1997) The definition of El Niño. Bulletin of the American Meteorological Society 78(12):2771–2777

Vecchi GA, Wittenberg AT (2010) El Niño and our future climate: where do we stand? Wiley Interdisciplinary Reviews: Climate Change 1:260–270, DOI 10.1002/wcc.33

Vecchi GA, Soden BJ, Wittenberg AT, Held IM, Leetmaa A, Harrison MJ (2006a) Weakening of tropical Pacific atmospheric circulation due to anthropogenic forcing. Nature 441, DOI 10.1038/nature04744

Vecchi GA, Wittenberg AT, Rosati A (2006b) Reassessing the role of stochastic forcing in the 1997-8 El Niño. Geophysical Research Letters 33:L01,706, DOI 10.1029/2005GL024738

Vialard J, Delecluse P (1998) An OGCM study for the TOGA decade. Part I: role of salinity in the physics of the western Pacific fresh pool. Journal of Physical Oceanography 28:1071–1088

Vialard J, Menkes C, Boulanger JP, Delecluse P, Guilyardi E, McPhaden MJ, Madec G (2001) A model study of oceanic mechanisms affecting equatorial Pacific sea surface temperature during the 1997-98 El Niño. Journal of Physical Oceanography 31(7):1649–1675

Voldoire A, Sanchez-Gomez E, Salas y Melia D, Decharme B, Cassou C, Senesi S, Valcke S, Beau I, Alias A, Chevallier M, Deque M, Deshayes J, Douville H, Fernandez E, Madec G, Maisonnave E, Moine MP, Planton S, Saint-Martin D, Szopa S, Tyteca S, Alkama R, Belamari S, Braun A, Coquart L, Chauvin F (2013) The CNRM-CM5.1 global climate model: description and basic evaluation. Climate Dynamics 40:2091–2121, DOI 10.1007/s00382-011-1259-y

Watanabe M, Suzuki T, O'Ishi R, Komuro Y, Watanabe S, Emori S, Takemura T, Chikira M, Ogura T, Sekiguchi M, Takata K, Yamazaki D, Yokohata T, Nozawa T, Hasumi H, Tatebe H, Kimoto M (2010) Improved climate simulation by MIROC5: Mean states, variability, and climate sensitivity. Journal of Climate 23(23):6312–6335, DOI 10.1175/2010JCLI3679.1

Watanabe M, Kug JS, Jin FF, Collins M, Ohba M, Wittenberg AT (2012) Uncertainty in the ENSO amplitude change from the past to the future. Geophysical Research Letters 39(L20703), DOI 10.1029/2012LG053305

Watanabe S, Hajima T, Sudo K, Nagashima T, Takemura T, Okajima H, Nozawa T, Kawase H, Abe M, Yokohata T, Ise T, Sato H, Kato E, Takata K, Emori S, Kawamiya M (2011) MIROC-

ESM: model description and basic results of CMIP5-20c3m experiments. Geoscientific Model Development Discussions 4(2):1063–1128, DOI 10.5194/gmdd-4-1063-2011

Wittenberg AT (2004) Extended wind stress analyses for ENSO. Journal of Climate 17:2526–2540, DOI 10.1175/1520-0442(2004)017<2526:EWSAFE>2.0.CO;2

Wittenberg AT (2009) Are historical records sufficient to constrain ENSO simulations? Geophysical Research Letters 36:L12,702, DOI 10.1175/JCLI3631.1

Wittenberg AT (2015) Low-frequency variations of ENSO. US CLIVAR variations 13(1):26–31

Wittenberg AT, Rosati A, Lau NC, Ploshay JJ (2006) GFDL's CM2 global coupled climate models. Part III: Tropical Pacific climate and ENSO. Journal of Climate 19:698–722, DOI 10.1175/JCLI3631.1

Wittenberg AT, Rosati A, Delworth TL, Vecchi GA, Zeng F (2014) ENSO modulation: Is it decadally predictable? Journal of Climate 27:2667–2681, DOI 10.1175/JCLI-D-13-00577.1

Wu T, Yu R, Zhang F, Wang Z, Dong M, Wang L, Jin X, Chen D, Li L (2010) The Beijing Climate Center atmospheric general circulation model: Description and its performance for the present-day climate. Climate Dynamics 34(1):123–147, DOI 10.1007/s00382-008-0487-2

Yang X, Vecchi GA, Gudgel RG, Delworth TL, Zhang S, Rosati A, Jia L, Stern WF, Wittenberg AT, Kapnick S, Msadek R, Underwood SD, Zeng F, Anderson W, Balaji V (2015) Seasonal predictability of extratropical storm tracks in GFDL's high-resolution climate prediction model. Journal of Climate 28:3592–3611, DOI 10.1175/JCLI-D-14-00517.1

Yeh SW, Park YG, Kirtman BP (2006) ENSO amplitude changes in climate change commitment to atmospheric CO_2 doubling. Geophysical Research Letters 33(L13711), DOI 10.1029/2005GL025653

Yeh SW, Kug JS, Dewitte B, Kwon MH, Kirtman BP, Jin FF (2009) El Niño in a changing climate. Nature 461:511–514, DOI 10.1038/nature08316

Yeh SW, Kug JS, An SI (2014) Recent progress on two types of El Niño: observations, dynamics, and future changes. Asia-Pacific Journal of Atmospheric Sciences 50(1):69–81, DOI 10.1007/s13143-014-0028-3

Yu JY, Kim ST (2013) Identifying the types of major el niño events since 1870. International Journal of Climatology 33(8):2105–2112, DOI 10.1002/joc.3575

Yukimoto S, Adachi Y, Hosaka M, Sakami T, Yoshimura H, Hirabara M, Tanaka TY, Shindo E, Tsujino H, Deushi M, Mizuta R, Yabu S, Obata A, Nakano H, Koshiro T, Ose T, Kitoh A (2012) A new global climate model of the Meterological Research Institute: MRI-CGCM3. Journal of the Meteorological Society of Japan 90A:23–64, DOI 10.2151/jmsj.2012-A02

Zhang Q, Kumar A, Xue Y, Wang W, Jin FF (2007) Analysis of the ENSO cycle in the NCEP coupled forecast model. Journal of Climate 40:1265–1284

Zhang W, Vecchi GA, Murakami H, Delworth TL, Wittenberg AT, Rosati A, Underwood SD, Anderson W, Harris L, Gudgel R, Lin SJ, Villarini G, Chen JH (2016) Improved simulation of tropical cyclone responses to ENSO in the western north Pacific in the high-resolution GFDL HiFLOR coupled climate model. Journal of Climate 29:1391–1415, DOI 10.1175/JCLI-D-15-0475.1